

1 **Transcriptional and electrophysiological aberrations in an induced pluripotent stem cell-derived**  
2 **model of spinocerebellar ataxia type 7**

3 LM Watson<sup>1,2†</sup>, DC Smith<sup>1,2†</sup>, JV Raimondo<sup>2,3,4†</sup>, RJ Burman<sup>2,3,4</sup>, R Ballo<sup>4</sup>, J Scholefield<sup>5</sup>, L Tyers<sup>4</sup>,  
4 SA Cowley<sup>6</sup>, MJA Wood<sup>1,7</sup>, SH Kidson<sup>2,4</sup>, LJ Greenberg<sup>1,2\*</sup>

5 <sup>1</sup>Division of Human Genetics, Department of Pathology, Faculty of Health Sciences, University of  
6 Cape Town, Cape Town, South Africa

7 <sup>2</sup>Institute of Infectious Disease and Molecular Medicine, Faculty of Health Sciences, University of  
8 Cape Town, Cape Town, South Africa

9 <sup>3</sup>Neuroscience Institute, Faculty of Health Sciences, University of Cape Town, Cape Town, South  
10 Africa

11 <sup>4</sup>Division of Cell Biology, Department of Human Biology, Faculty of Health Sciences, University of  
12 Cape Town, Cape Town, South Africa

13 <sup>5</sup>Gene Expression & Biophysics Group, Synthetic Biology ERA, CSIR Biosciences, Pretoria, South  
14 Africa

15 <sup>6</sup>Sir William Dunn School of Pathology, University of Oxford, Oxford, United Kingdom

16 <sup>7</sup>Department of Physiology, Anatomy and Genetics, University of Oxford, Oxford, United Kingdom

17 †These authors contributed equally to this work.

18 \***Correspondence:** LJ Greenberg: [jacque.greenberg@uct.ac.za](mailto:jacque.greenberg@uct.ac.za)

19 **Keywords:** cellular electrophysiology, induced pluripotent stem cells, transcriptomics, spinocerebellar  
20 ataxia type 7

21 **Abstract**

22 Spinocerebellar ataxia type 7 (SCA7) is an inherited neurodegenerative disease that is characterised by  
23 ataxia and visual loss. It results from a degeneration of cerebellar Purkinje neurons and retinal  
24 photoreceptors caused by a polyglutamine repeat expansion in the ATXN7 gene, a component of the  
25 STAGA transcription co-activator complex. As with many neurodegenerative diseases, studies of  
26 pathogenesis have been hindered by a lack of disease-relevant models. To this end, we have generated  
27 the first induced pluripotent stem cells (iPSCs) from South African SCA7 patients, where the disease  
28 occurs at an unusually high frequency as a result of a founder effect. These iPSCs were capable of  
29 differentiation into neural and retinal cells, and showed evidence of a transcriptional phenotype  
30 affecting components of STAGA (*ATXN7* and *KAT2A*) and the heat shock protein pathway (*DNAJ1*  
31 and *HSP70*). Functionally, SCA7 iPSC-derived neurons exhibited more negative resting membrane  
32 potentials and increased input resistance compared to controls, suggesting reduced excitability in  
33 response to synaptic input. These results provide the first evidence of a disease phenotype in SCA7  
34 iPSC-derived cells, establishing a valuable model for the study of neurodegenerative diseases and the  
35 development of population-specific therapies.  
36

## 37 **1. Introduction**

38 Spinocerebellar ataxia type 7 (SCA7) is an inherited neurodegenerative disease caused by a CAG  
39 repeat expansion in the *ATXN7* gene. Since the translation of this CAG repeat leads to an expanded  
40 polyglutamine (polyQ) tract within the resultant protein, SCA7 is classified as a polyQ-repeat disorder.  
41 Other diseases with a similar pathophysiology include five different SCAs (SCA 1, 2, 3, 6 and 17), as  
42 well as Huntington disease, dentatorubral-pallidoluysian atrophy and spinal bulbar muscular atrophy  
43 (Orr and Zoghbi, 2007).

44 Clinically, SCA7 patients present with ataxia, dysarthria and visual loss. This is caused by a selective  
45 degeneration of cerebellar Purkinje neurons and retinal photoreceptors (Gouw et al., 1994). Symptoms  
46 progressively worsen over a period of 10 to 30 years, leading ultimately to brainstem dysfunction,  
47 blindness, physical disability and death.

48 The mechanism by which a polyQ expansion within the ubiquitously expressed *ATXN7* protein leads  
49 to the selective degeneration of Purkinje neurons and photoreceptors remains to be fully elucidated.  
50 *ATXN7* is known to be a component of the mammalian transcription co-activator complex, STAGA  
51 (SPT3-TAF9-ADA-GCN5 acetyltransferase) (Garden and La Spada, 2008), and has been shown to  
52 facilitate interaction between STAGA and the cone-rod homeobox (CRX) transactivator of  
53 photoreceptor genes, linking the function of *ATXN7* with the retinal phenotype observed in SCA7  
54 patients (Palhan et al., 2005). In neuronal cells, several studies have highlighted the role of  
55 transcriptional aberrations in the dysfunction that precedes the onset of disease symptoms (Palhan et  
56 al., 2005, Ström et al., 2005, Abou-Sleymane et al., 2006, Garden and La Spada, 2008, Chou et al.,  
57 2010). These gene expression changes may arise either directly from alterations in transcriptional  
58 regulation by mutant *ATXN7*, or indirectly, as a consequence of a generalised cellular response to the  
59 presence of mutant *ATXN7*.

60 As with many neurodegenerative conditions, research into the molecular pathogenesis of SCA7 has  
61 been hindered by a lack of suitable models of human disease progression. This is particularly relevant  
62 in cases where the genomic context of the mutation may have an impact on gene function and might  
63 prove useful for therapeutic development. SCA7 occurs at an unusually high frequency in the South  
64 African population as a result of a founder effect in patients of Black African ethnic origin (Smith et  
65 al., 2012, Smith et al., 2016). South African SCA7 patients also display a unique phenomenon – a  
66 single nucleotide polymorphism (SNP) within *ATXN7* (rs3774729), which is linked to the mutation in  
67 all patients studied to date (Greenberg et al., 2006). Approximately 43% of these individuals are  
68 heterozygous for the polymorphism, allowing for allelic discrimination, and providing an ideal target  
69 for developing an allele-specific silencing therapy. Recently, this haplotype has been shown to extend  
70 into other Southern African populations, suggesting that such a therapy may be more widely  
71 \*\*\*\*applicable than was first thought (Smith et al., 2015). We have previously demonstrated the  
72 efficacy of an allele-specific RNAi treatment in an over-expression cell model of SCA7 (Scholefield  
73 et al., 2009), as well as in SCA7 patient fibroblasts (Scholefield et al., 2014). Disease-relevant cell  
74 lines generated from these patients are thus of vital importance in the understanding of disease  
75 pathogenesis and the development of therapies, as they carry the patient's full genomic sequence,  
76 including SNPs which may be used as targets for gene silencing.

77 In this study, we have generated and characterised multiple induced pluripotent stem cell (iPSC) lines  
78 from two South African SCA7 patients and an unaffected, related control. The generation of iPSCs  
79 involves reprogramming somatic cells to a pluripotent state by means of viral transduction with the  
80 pluripotency genes *OCT4*, *SOX2*, *KLF4* and *c-MYC* (Takahashi and Yamanaka, 2006, Takahashi et al.,

81 2007). Importantly, iPSCs can then be differentiated into any tissue of the body through treatment with  
82 specific growth factors, making them a useful starting point for the generation of disease-relevant cell  
83 models, particularly in neurodegenerative diseases, where primary CNS cultures may only be obtained  
84 using invasive methods. We have successfully differentiated SCA7 patient and control iPSCs into cells  
85 expressing markers associated with retinal photoreceptors, neural progenitors and neurons.  
86 Furthermore, we have obtained preliminary evidence for a disease phenotype in these cells, in the form  
87 of pathogenically relevant gene expression changes and alterations in intrinsic neuronal properties.  
88 These cells may thus provide a highly relevant model in which to screen potential therapeutic  
89 modalities, by monitoring the effect of such therapies on disease manifestations *in vitro*.

## 90 **2. Methods**

### 91 **Ethics approval and patient recruitment**

92 Ethics approval for the study was granted by the University of Cape Town (UCT) Faculty of Health  
93 Sciences Human Research Ethics Committee (HREC REF. 380/2009 and 434/2011), and was renewed  
94 annually, incorporating amendments to the project protocol where necessary. All methods were carried  
95 out in accordance with the guidelines approved by the Ethics Committee. Participants were recruited  
96 from the Neurogenetics clinic at Groote Schuur Hospital in Cape Town. Informed consent was obtained  
97 from all participants prior to their enrolment in the study.

### 98 **Establishment of primary fibroblast cultures**

99 Primary fibroblast cultures were established from punch skin biopsies taken from the inner forearm of  
100 two unrelated SCA7 patients (P1 and P2) and an unaffected control individual (C1, sibling of P2) who  
101 had consented to participate in the study, as previously described (Freshney, 2000). CAG genotypes  
102 and ages at diagnosis and biopsy are reflected in **Table S-1.1**.

### 103 **Generation and characterisation of patient-derived iPSCs**

104 Reprogramming of dermal fibroblasts into iPSCs was achieved through the introduction of Sendai virus  
105 vectors (SeVdp) containing *OCT4*, *SOX2*, *KLF4* and *c-MYC* as previously described (Nishimura et al.,  
106 2011, Nakanishi and Otsu, 2012). The expression of pluripotency markers OCT4 and TRA-1-60, as  
107 well as silencing of the reprogramming Sendai virus, were confirmed by immunocytochemistry  
108 (antibodies listed in **Table S-1.2**). The expression of selected pluripotency genes (*OCT4*, *SOX2*,  
109 *NANOG*) was determined by quantitative PCR (see below). Genomic integrity was assessed by means  
110 of karyotype analysis (G-banding). To confirm the iPSC lines' capacity to differentiate into the three  
111 embryonic germ layers, *in vitro* differentiation via embryoid body formation was performed as  
112 previously described (Martl et al., 2013).

### 113 **Neural differentiation and characterisation**

114 Differentiation of iPSCs into neural precursors was performed by treatment of iPSCs with 3 $\mu$ M  
115 glycogen synthase kinase 3 (GSK3) inhibitor (CHIR99021) and 2 $\mu$ M TGF $\beta$  inhibitor (SB431542) as  
116 previously described (Li et al., 2011). For neuronal differentiation, neural precursors were seeded at a  
117 density of 150 000 cells/well onto a Matrigel-coated six-well plate in neural induction medium (Li et  
118 al., 2011). After two days, medium was changed to neuronal differentiation medium supplemented  
119 with N2, B27, 300ng/ml cyclic AMP (Sigma), 0.2mM ascorbic acid (Sigma), 10ng/ml BDNF  
120 (Peprotech) and 10ng/ml GDNF (Peprotech) and cells were maintained in culture for 14 to 21 days.

121 Characterisation was performed by immunocytochemistry and qPCR (for antibodies and primers, see  
122 **Tables S-1.2 and S-1.3**).

### 123 **Electrophysiology**

124 Neurons maintained on glass cover slips were removed from the incubator and rapidly transported to  
125 the recording chamber of a Zeiss Axioskop Upright Microscope (Zeiss). Electrophysiological  
126 recordings were made in neuronal differentiation medium at room temperature and were restricted to  
127 the first 5 hours following cell removal from the incubator environment. Patch pipettes of 13-20 M $\Omega$   
128 tip resistance were pulled from filamental borosilicate glass capillaries (2.00 mm outer diameter, 1.58  
129 mm inner diameter, Hilgenberg), using a horizontal puller (Model P-1000, Sutter). The pipettes were  
130 filled with an internal solution containing (in mM): K-gluconate (126); KCl (4); Na<sub>2</sub> ATP (4); NaGTP  
131 (0.3); Na<sub>2</sub>-phosphocreatinine (10) and HEPES (10). Osmolarity was adjusted to between 290 and 300  
132 mOsM and the pH was adjusted to between 7.38 and 7.42 with KOH. Cells were visualised using a  
133 40x water-immersion objective (Zeiss). Digital images were obtained using a CCD camera (VX55,  
134 TILL Photonics). Individual cells were selected for recordings based on a small round or ovoid cell  
135 body (diameters, 5–10  $\mu$ m) and typically two or more extended processes. Recordings were made in  
136 current clamp and voltage clamp mode using an Axopatch 200B amplifier (Molecular Devices). Data  
137 acquisition was performed through an ITC-1600 board (Instrutech) connected to a PC running a  
138 custom-written routine (PulseQ) under IGOR Pro (Wavemetrics). Analysis was performed using  
139 custom-written scripts in MATLAB (Mathworks).

### 140 **Retinal differentiation and characterisation**

141 Differentiation into retinal photoreceptors was performed as previously described (Boucherie et al.,  
142 2013), using iPSCs cultured in feeder-free conditions on Matrigel in mTESR<sup>TM</sup> medium. The cells  
143 were dissociated enzymatically and plated onto Matrigel-covered dishes in neural differentiation  
144 medium containing N2 and B27 supplements (Life Technologies). After settling for an hour, adhered  
145 cells were covered in a 2% Matrigel solution. The following day the medium was replaced with neural  
146 differentiation medium without Matrigel, and cells were fed with fresh medium every second day.  
147 From day 10 the medium was supplemented with 3nM recombinant SHH (R&D Systems), 50ng/ $\mu$ l  
148 acidic fibroblast growth factor (aFGF) (R&D Systems), 10ng/ $\mu$ l basic fibroblast growth factor (bFGF)  
149 (Miltenyi), 1mM taurine and 500nM retinoic acid (both Sigma Aldrich). Characterisation was  
150 performed by immunocytochemistry and qPCR (for antibodies and primers, see **Tables S-1.2 and S-**  
151 **1.3**).

### 152 **DNA and RNA isolation, cDNA synthesis**

153 DNA extraction from cultured cells was performed using the QIAGEN DNeasy Blood and Tissue Kit.  
154 RNA was isolated from cultured cells using the QIAGEN RNeasy Plus Mini Kit. Synthesis of cDNA  
155 was performed using the Applied Biosystems High Capacity cDNA Reverse Transcription Kit (Life  
156 Technologies) using 500ng-1 $\mu$ g template RNA.

### 157 **Real-time quantitative PCR**

158 Real-time quantitative PCR (qPCR) was performed on the BioRad CFX96 Real-Time PCR System,  
159 using the Power SYBR Green PCR Master Mix (Applied Biosystems), according to manufacturer's  
160 instructions. Primers (**Table S-1.2**) were obtained from PrimerDesign Ltd, Integrated DNA  
161 Technologies (IDT), or Sigma-Aldrich.

162 Relative quantities of target mRNA were determined using the relative standard curve method  
163 (Larionov et al., 2005). Standard curves were prepared for each primer pair, from serial dilutions of  
164 pooled sample cDNA. Universal cycling conditions were used (95°C for 10min, followed by 40 cycles  
165 of 95°C for 15 seconds and 60°C for 1min). PCRs were performed in technical triplicate, on at least  
166 two biological replicates, and results were analysed using the BioRad CFX Manager software (v3.1).  
167 Gene of interest expression was normalised to *beta actin* (*ACTB*) expression in each case. The design  
168 and reporting of qPCR experiments aimed to comply with the Minimum Information for publication  
169 of Quantitative real-time PCR Experiments guidelines (Taylor et al., 2006, Bustin et al., 2009)  
170 wherever possible. Statistical analysis was performed using the Students' t-test (two-tailed, assuming  
171 unequal variances). Significance was defined as  $p < 0.05$ .

## 172 CAG repeat length determination

173 The length of the disease-causing CAG repeat in *ATXN7* was determined from DNA by means of  
174 polymerase chain reaction (PCR) and automated fluorescent genotyping. The PCR reaction mix  
175 consisted of 0.4µM each, forward and reverse primer (**Table S-1.1**), 0.6units of GoTaq DNA  
176 polymerase (Promega), 100ng of DNA, and Failsafe buffer J (Epicentre Biotechnologies) at a final  
177 concentration of 1X, made up to a final reaction volume of 10µl. Cycling conditions were as follows:  
178 95°C for 5min; followed by 30 cycles of 95°C for 30 seconds, 53°C for 6 seconds and 72°C for 40  
179 seconds; and a final elongation step at 72°C for 7min. Automated fluorescent genotyping was  
180 performed using the ABI 3130xl Genetic Analyzer (Applied Biosystems).

181 The length of the CAG repeat [(CAG)<sub>n</sub>] was approximated using the following equation, adapted from  
182 (Dorschner et al., 2002):  $n = \frac{(0.3063 \times \text{Length of major PCR product in base pairs}) - 76.475\text{bp}}{29.7}$ . The  
183 major PCR product was defined as the product generating the highest fluorescent peak, as detected  
184 using the ABI 3130xl Genetic Analyzer.

## 185 3. Results

### 186 Generation and characterisation of iPSCs

187 Following Sendai virus-mediated reprogramming, iPSC colonies with the correct morphology (flat,  
188 with distinct borders, containing tightly packed cells with a high nucleus-to-cytoplasm ratio) appeared  
189 within three to four weeks (**Figure 1a**). These colonies were manually picked and clonally expanded  
190 in separate dishes on a feeder layer of inactivated mouse embryonic fibroblasts. Three SCA7 patient  
191 iPSC lines and two control lines (representing two affected individuals and a single related, unaffected  
192 control) were successfully generated and characterised (**Table S-1.1**).

193 Immunocytochemical analysis of SCA7 patient and control iPSC lines revealed iPSC colonies with  
194 distinct nuclear staining for the pluripotency transcription factor, OCT4, compared to the surrounding  
195 mouse embryonic feeder fibroblasts (**Figure 1b**). The iPSC colonies also stained positive for the  
196 embryonic stem cell surface marker TRA-1-60 (**Figure 1b**).

197 The expression of pluripotency markers was further confirmed by qPCR. All five iPSC lines expressed  
198 high levels of *OCT4*, *SOX2* and *NANOG*, standard markers of pluripotency (**Figure 1c**), compared to  
199 donor fibroblasts or cells that had been subjected to retinal or neuronal differentiation. The expression  
200 levels of *SOX2* and *NANOG* were similar across the five iPSC lines, but lines P2b and C1b showed  
201 lower levels of *OCT4* expression compared to the remaining three lines (although still significantly  
202 higher than differentiated fibroblasts and retinal cells).

203 Co-staining of all iPSC lines with primary antibodies against OCT4 and the nucleocapsid protein of  
204 the virus (anti-NP) showed little or no evidence of NP staining in the OCT4-positive pluripotent cells



205 (**Figure 1d**, bottom panel), compared to intense cytoplasmic staining in newly infected fibroblasts  
206 (**Figure 1d**, top panel). This indicated that the Sendai virus had been effectively silenced, and that the  
207 iPSCs had achieved self-regulating pluripotency. All lines were assessed after passage 8.

208  
209 *In vitro* embryoid body-mediated differentiation confirmed the ability of all five lines to differentiate  
210 into the three embryonic germ layers, staining positive for forkhead box A2 (FOXA2) or alpha-  
211 fetoprotein (AFP) (endoderm); sarcomeric alpha actinin (ASA) or smooth muscle actin (SMA)  
212 (mesoderm); and glial fibrillary acidic protein (GFAP) or  $\beta$ III-tubulin (ectoderm) (**Figure 1e**).

213  
214 Karyotyping using standard G-banding analysis revealed no gross structural abnormalities, when iPSC  
215 lines were compared to the fibroblasts from which they had been derived (**Figure S-1.1**).

## 216 **Neural differentiation of iPSCs**

217 SCA7 patient and control iPSCs generated neural precursor cells (NPCs) at comparable efficiencies,  
218 when cultured in neural induction medium supplemented with SB431542 (TGF $\beta$  inhibitor) and  
219 CHIR99021 (GSK3 inhibitor), with 100% of the cells expressing the early neural marker Nestin, after  
220 five passages (**Figure 2a**). The cells also stained positive for the disease-causing protein, ATXN7  
221 (**Figure 2b**), and demonstrated repression of the pluripotency gene *OCT4*, and upregulation of the early  
222 neural gene *PAX6* (**Figure 2c**).

223 After culture for 14 days in neuronal differentiation medium containing N2/B27 supplement, cAMP  
224 ascorbic acid, BDNF and GDNF (Li et al., 2011), both SCA7 patient and control NPCs stained positive  
225 for the neuronal marker  $\beta$ III-Tubulin, and showed robust, diffuse nuclear localisation of the disease-  
226 causing protein, ATXN7 (**Figure 2d**). A subset of cells (approximately 1.8%) stained positive for  
227 gamma-aminobutyric acid (GABA), although the proportion of GABAergic neurons did not appear to  
228 vary between SCA7 patients and controls (**Figure 2d**). No obvious differences in morphology were  
229 observed when comparing neurons derived from SCA7 patient iPSCs with those derived from controls.

230 Cells were assayed for physiological properties between 14 and 23 days post induction of neuronal  
231 differentiation. Cells were targeted for whole-cell recordings based on their morphological properties.  
232 This included a small round or ovoid cell body with diameters between 5–10  $\mu$ m and typically two or  
233 more extended processes (see **Figure 3a**). Following the attainment of a whole-cell patch, current  
234 pulses of between 0 and 10 pA were applied. Individual cells displayed four general types of spiking  
235 responses: a purely passive (**Figure 3a**), abortive spike (**Figure 3b**), single spike (**Figure 3c**) and  
236 recurrent spiking response (**Figure 3d**). These spiking properties are similar to those observed in acute  
237 human fetal brain slices (Moore et al., 2009), hESC-derived neurons (Perrier et al., 2004; Vazin et al.,  
238 2009; Belinsky et al., 2011) and iPSC-derived neurons (Belinsky et al., 2014). A postmitotic neuron  
239 matures by inserting voltage-gated channels into its plasma membrane (Moody and Bosma, 2005).  
240 Therefore the spiking response of a cell to current injection can be used to determine the maturation  
241 stage of a differentiating neuron: passive (least mature)  $\rightarrow$  abortive spike  $\rightarrow$  single spike  $\rightarrow$  recurrent  
242 spikes (most mature).

243 Spiking responses were collected in current-clamp mode from cells derived from four separate iPSC  
244 lines: two control lines C1a (n = 42) and C1b (n = 69), and two patient lines P1a (n = 44) and P2b (n =  
245 72). Although the fraction of cells which fell into each spiking response category was significantly  
246 dependent on the iPSC line from which the cells were derived (p<0.0001, Chi-squared test), no trend  
247 could be discerned between control and patient lines (see **Figure 3e**). For example, the control line  
248 C1b had the most mature phenotype with the highest fraction of cells in the single spike and recurrent

249 spiking categories whilst P2b demonstrated a relatively immature phenotype, with the majority of cells  
250 displaying spiking responses falling into the passive category. However, this difference was not  
251 corroborated by the other lines where the control line C1a displayed a less mature phenotype than  
252 patient line P1a. The maximum number of spikes that could be elicited following current injection was  
253 again significantly dependent on the cell line concerned. Mean values  $\pm$  SEM for each line were: C1a  
254 0.5  $\pm$  0.1, C1b 1.3  $\pm$  0.2, P1a 1.0  $\pm$  0.3 and P2b 0.4  $\pm$  0.1 spikes, see **Figure 3f**,  $p < 0.0001$ ,  
255 ANOVA. However, no consistent trend could be observed between cells derived from control versus  
256 patient iPSC lines.

257 Next, we compared the resting membrane potential ( $V_m$ ) of cells derived from each cell line. This  
258 parameter was significantly dependent on the iPSC line from which the cells were derived (see **Figure**  
259 **3g**,  $p = 0.0004$ , ANOVA). The mean resting membrane potential  $\pm$  SEM for the C1a, C1b, P1a and  
260 P2b cell lines were -54.7  $\pm$  3.1, -57.0  $\pm$  1.7, -67.4  $\pm$  2.8 and -67.3  $\pm$  2.7 mV respectively. The  
261 control lines had significantly more depolarised resting membrane potentials as compared to patient  
262 derived cell lines ( $p < 0.0001$ , t-test).

263 We then determined the input resistance of each cell. A lower input resistance is associated with neurite  
264 outgrowth and increased numbers of ion channels inserted into the plasma membrane during the  
265 process of neuronal maturation. Once again, a cell's input resistance was significantly dependent on  
266 the cell line to which it belonged (see **Figure 3h**,  $p = 0.0012$ , ANOVA). Input resistance  $\pm$  SEM was  
267 4987  $\pm$  421, 5484  $\pm$  243, 5979  $\pm$  513 and 7094  $\pm$  455 m $\Omega$  for the C1a, C1b, P1a and P2b cell  
268 lines respectively. Cells derived from patient lines had a significantly higher mean input resistance than  
269 cells from the control lines ( $p = 0.0005$ , t-test).

270 Following our assessment of the active and passive properties of cells described above, we then directly  
271 measured voltage-gated sodium and potassium currents in voltage-clamp mode (**Figure 4a,b** and **c**).  
272 As one would predict, the spiking properties of neurons are directly correlated with the size of their  
273 currents. Indeed we found a significant correlation between the maximum number of spikes that could  
274 be elicited in a cell and the size of its subsequently measured voltage-gated sodium and potassium  
275 currents (data not shown,  $r = -0.62$  and  $0.36$  for voltage-gated sodium and potassium currents  
276 respectively,  $p < 0.0001$  for both, Pearson correlation).

277 The maximum size of voltage-gated sodium currents and potassium currents measured in each cell  
278 (Max.  $I_{Na}$  and Max.  $I_K$ ) was significantly dependent on the particular iPSC line concerned (see **Figure**  
279 **4d** and **e**,  $p < 0.0001$  in both cases, ANOVA). The mean Max.  $I_{Na}$   $\pm$  SEM was -166.5  $\pm$  18.6, -277.1  
280  $\pm$  23.0, -268.0  $\pm$  30.5 and -108.0  $\pm$  14.2 pA for the C1a, C1b, P1a and P2b cell lines. The mean  
281 Max.  $I_K$   $\pm$  SEM was 180.1  $\pm$  16.5, 176  $\pm$  10.8, 222.5  $\pm$  19.3 and 105.7  $\pm$  8.0 pA for the C1a,  
282 C1b, P1a and P2b cell lines respectively. Similar to what was observed for the spiking responses, there  
283 was no consistent trend in the size of voltage-gated currents between cells derived from control as  
284 compared to iPSC lines.

## 285 **Retinal differentiation of iPSCs**

286 For the retinal differentiation of iPSCs, the Matrigel "sandwich" system facilitated a rapid self-  
287 organisation and differentiation of the pluripotent stem cells into structures containing cells  
288 morphologically indicative of columnar neuroepithelia (**Figure 5a**, first image). These structures lost  
289 their integrity from day 4-5, and cells spread into an adherent monolayer (**Figure 5a**, middle image).  
290 The gradual emergence of cells with a neuronal morphology was observed from day 10 to day 30,  
291 particularly in areas of low confluence (**Figure 5a**, last image). Following differentiation of patient

292 and control cells into retinal cells, immunocytochemical analyses were performed on cells at the end  
293 of the differentiation period (day 30), to determine whether the cells expressed retinal cell markers.  
294 The cells were stained for either the disease-causing protein ATXN7, or the retinal cell markers CRX  
295 and RCVRN (**Figure 5b**). No obvious differences in morphology were observed between SCA7 patient  
296 and control-derived cells. The differentiated cells displayed varying expression levels of the retinal  
297 genes *CRX*, *PAX6*, *RCVRN* and *OTX2* (**Figure 5a and c**).

### 298 **CAG repeat length**

299 In order to confirm the size of the *ATXN7* CAG repeat alleles in mRNA from patient- and control-  
300 derived fibroblasts, iPSCs, NPCs and retinal cells, an RT-PCR-based assay was performed. The results  
301 were visualised on an agarose gel (**Figure S-1.2a and b**), and confirmed by automated fluorescent  
302 genotyping (data not shown). The length of the CAG repeat did not appear to fluctuate during  
303 reprogramming or differentiation, corresponding to previous reports in similar cell lines (Camnasio et  
304 al., 2012, Koch et al., 2011). This assay also confirmed that both the mutant and wild-type *ATXN7*  
305 alleles were expressed by all cell types, and that there were no obvious differences in allele expression  
306 in affected or unaffected cells.

### 307 **Transcriptional dysregulation**

308 To determine whether any transcriptional differences could be detected between SCA7 patient- and  
309 unaffected control-derived cell types, a panel of candidate genes was selected, which had previously  
310 been shown to be dysregulated in the retinal and cerebellar tissue of SCA7 mouse models and patient  
311 lymphoblasts (Yoo et al., 2003, Tsai et al., 2005, Abou-Sleymane et al., 2006, Chou et al., 2010). The  
312 panel included the following genes: *ATXN7*, brain expressed, X-linked 1 (*BEX1*), DnaJ (Hsp40)  
313 homolog, subfamily A, member 1 (*DNAJ1*), glutamate receptor, ionotropic, AMPA 2 (*GRIA2*), heat  
314 shock protein 27 (*HSP27*), heat shock protein 70 (*HSP70*), heat shock protein 105 (*HSP105*),  
315 oligodendrocyte transcription factor 1 (*OLIG1*), Phospholipase C, Beta 3 (*PLCB3*) and ubiquitin  
316 carboxyl-terminal esterase L1 (*UCHL1*). The expression of these genes was determined in fibroblasts,  
317 iPSCs, NPCs and retinal cells by means of qPCR. The expression of an additional panel of retinal  
318 genes was evaluated in the iPSC-derived retinal cells, including arrestin 3 (*ARR3*), cone-rod homeobox  
319 (*CRX*), guanine nucleotide binding protein (G protein), alpha transducing activity polypeptide 1  
320 (*GNAT1*), Microphthalmia-associated transcription factor (*MITF*), neural retina leucine zipper (*NRL*),  
321 orthodenticle homeobox 2 (*OTX2*), paired box 6 (*PAX6*), recoverin (*RCVRN*), rhodopsin (*RHO*) and  
322 retinal pigment epithelium-specific protein 65kDa (*RPE65*).

323 No consistent, significant alterations in gene expression were observed between SCA7 patient and  
324 control fibroblasts or undifferentiated iPSCs (**Figure S-1.3**), highlighting the need to investigate  
325 neurodegenerative phenotypes in disease-relevant differentiated cell types.

326 In contrast to the fibroblasts and undifferentiated iPSCs, several genes were found to be significantly  
327 differentially expressed between SCA7 patient iPSC-derived retinal cells and NPCs, when compared  
328 to the equivalent cell type derived from unaffected control lines. Two genes were consistently  
329 downregulated in both retinal cells and NPCs. These included the disease-causing gene *ATXN7* ( $p =$   
330  $0.018$ , NPCs,  $p = 0.04$ , retinal photoreceptors); and the K (lysine) acetyltransferase 2A (*KAT2A*),  
331 encoding GCN5, the histone acetyltransferase (HAT) component of the STAGA transcription  
332 coactivator complex ( $p = 0.003$ , NPCs,  $p = 0.02$ , retinal photoreceptors) (**Figure 6**).

333 Six genes were differentially expressed in either SCA7 patient photoreceptors or NPCs, but not both.  
334 Those specific to SCA7 photoreceptors included *GRIA2*, encoding the glutamate receptor, ionotropic,  
335 AMPA2 (GluR2) (downregulated,  $p = 0.04$ ); and three retinal-specific genes, *OTX2* (upregulated,  $p =$   
336  $0.002$ ), *RCVRN* (downregulated,  $p = 0.01$ ) and *RPE65* (upregulated,  $p = 0.001$ ), which were not



337 assessed in NPCs. NPC-specific alterations in expression were identified in the heat shock protein  
338 genes *DNAJ1* ( $p = 0.04$ ) and *HSP70* ( $p = 0.04$ ), both of which were found to be downregulated in  
339 SCA7-patient derived cells.

340 Finally, *BEX1*, an interactor of the p75 neurotrophin receptor, which regulates neurotrophin signalling  
341 and neuronal differentiation, was found to be upregulated in SCA7 photoreceptors ( $p=0.0006$ ), and  
342 downregulated in SCA7 NPCs ( $p = 0.03$ ), indicative of a possible differential response by the different  
343 cell types to the presence of mutant ATXN7.

344 As expected, a considerable degree of intra- and inter-individual variability was observed, with some  
345 genes showing significant changes in gene expression in one SCA7 patient line, but not another. Given  
346 the small number of lines used, however, emphasis was placed on those genes showing robust  
347 alterations in expression across all patient lines assessed.

#### 348 349 **4. Discussion**

350 This study describes the generation and characterisation of the first iPSCs from the South African  
351 SCA7 patient cohort, through the transduction of patient dermal fibroblasts with Sendai viral vectors  
352 (Nishimura et al., 2011, Nakanishi and Otsu, 2012), as well as the differentiation of these iPSCs into  
353 neurons and retinal photoreceptors. This is the first report to include multiple patients, and to  
354 demonstrate a phenotype in disease-relevant cell types. To our knowledge, it is only the second report  
355 of iPSCs generated from SCA7 patients (Luo et al., 2012).

356 The SCA7 patient iPSCs generated in this study were shown to be able to differentiate into a  
357 homogeneous population of NPCs, capable of self-renewal for up to 30 passages, and with  
358 morphological similarities to neuroepithelial cells, as has been previously reported (Li et al., 2011).  
359 The generation of sustainable populations of neural precursors from SCA7 patients is significant, as  
360 these cells may act as a starting point for the generation of numerous disease-affected neuronal  
361 subtypes, which can be expanded for large-scale experiments at relatively low cost.

362 Both patient- and control- derived NPCs appeared capable of differentiating into neurons expressing  
363  $\beta$ III-Tubulin and GABA, with comparable efficiencies. This corresponds with results from previous  
364 studies of neurodegenerative conditions, including other polyQ diseases (Soldner et al., 2009, Koch et  
365 al., 2011, Camnasio et al., 2012), which found no difference in differentiation potential between patient  
366 and control iPSCs. In addition, no obvious difference in the ability to generate GABA-positive  
367 processes could be detected between SCA7 and control iPSC-derived neurons.

368 Electrophysiological studies were carried out to establish whether there were any functional differences  
369 in the intrinsic properties of patient and control cells. The majority of cells recorded were capable of  
370 generating spiking activity including single and multiple action potentials, an indication of neuronal  
371 maturity (Moody and Bosma, 2005). Despite the presence of significant differences in spiking  
372 responses between the four cell lines, we did not observe a reliable trend between the control and  
373 patient derived neurons. This is consistent with our observations of voltage-gated sodium and  
374 potassium currents, which underlie spiking activity. Significant variability, perhaps due to  
375 unappreciated differences in culturing conditions between cell lines, may have masked our ability to  
376 detect a reliable difference in spiking responses due to mutant ATXN7. Alternatively, it may be that  
377 mutant ATXN7 does not affect the spiking properties of neurons at early stages of development,  
378 suggesting that an extrinsic stressor of some kind might be required to elicit a pathological phenotype.  
379 Indeed, similar functional analysis of neurons derived from patients with SCA3, a related polyQ-repeat  
380 disorder, showed no difference between control and patient cells until neurons were excited via bath  
381 application of glutamate (Koch et al., 2011).

382 Importantly, we did observe differences in resting membrane potential and input resistance between  
383 control and SCA7 patient derived neurons. Patient cells had more negative resting membrane potentials  
384 and increased input resistance compared to control cells. Both of these differences would serve to  
385 reduce the excitability of neurons containing mutant ATXN7 in response to synaptic input. Reductions  
386 in Purkinje cell excitability have previously been observed in animal models of SCA1 and SCA2  
387 (Duvick et al., 2010, Hansen et al., 2012) and could represent a common functional endpoint in several  
388 polyQ disorders (Choppra et al., 2014). Future work will involve exploring the underlying mechanisms  
389 which might explain these differences in resting membrane potential and input resistance. Importantly,  
390 it will be necessary to repeat this physiological functional analysis on iPSC derived neurons of the  
391 Purkinje cell lineage in order to fully recapitulate the cerebellar-specific elements of the disease using  
392 the recently published protocols (Muguruma, 2017, Watson et al., 2018).

393 Retinal differentiation of iPSCs yielded a heterogeneous cell population after 30 days, containing a  
394 large proportion of cells expressing the photoreceptor markers CRX and RCVRN, as well as retinal  
395 cell genes *PAX6*, *OTX2*, *CRX* and *NRL* in the differentiating cells. The cells expressed varying levels  
396 of the photoreceptor genes, *RCVRN* and *RHO*, confirming that the retinal differentiation protocol was  
397 capable of producing cells expressing markers of "mature" photoreceptors, albeit at relatively low  
398 levels of efficiency.

399 A PCR-based assay was used to confirm the size of the *ATXN7* CAG repeat alleles in cDNA from  
400 patient- and control-derived fibroblasts, iPSCs, neural and retinal cells. Besides serving as a  
401 "fingerprinting" assay, confirming the identity of the lines, these results offered a semi-quantitative  
402 analysis of the expression levels of mutant and wildtype *ATXN7* alleles, confirming that both alleles  
403 were expressed at approximately equal levels in all cell lines. Despite the inherent instability of the  
404 CAG repeat within the *ATXN7* gene (Monckton et al., 1999), automated fluorescent genotyping of the  
405 PCR products indicated that no contractions or large-scale expansions had occurred during either  
406 reprogramming or differentiation, consistent with previous reports of other iPSC-derived models of  
407 polyQ disorders, including SCA3 and HD (Koch et al., 2011, Camnasio et al., 2012).

408 Immunocytochemical analysis of ATXN7 expression in SCA7 patient neural and retinal cells showed  
409 diffuse expression within the nucleus (neurons) or nucleus and cytoplasm (retinal photoreceptors). No  
410 obvious intranuclear inclusions were observed in either the iPSCs or the differentiated cells. This  
411 strongly suggests that the differentiated cells represent a population of cells at an early stage of  
412 development, rather than recapitulating the age or disease stage of the patient from which the primary  
413 cells were derived. Previous studies employing similar models for the study of neurodegenerative  
414 disease have raised concerns regarding the relevance of modelling adolescent- and adult-onset diseases  
415 over the short lifespan of cultured neurons, suggesting that pathological hallmarks of disease such as  
416 the formation of aggregates may take decades to manifest, requiring the gradual accumulation of toxic  
417 proteins as a result of age-dependent deficiencies in protein homeostasis (Soldner et al., 2009, Hartl et  
418 al., 2011). Although some studies suggest that aggregates may be detected at earlier stages, the major  
419 determinants of aggregate formation remain the length of the polyQ expansion, and the levels of  
420 expression of the polyQ-containing protein (Miller et al., 2010, Arrasate et al., 2004). Thus, a cell line  
421 derived from an individual expressing endogenous levels of a moderately expanded ATXN7 protein  
422 may be less likely to demonstrate an observable cellular phenotype. Alternatively, the aggregation of  
423 mutant protein may require prolonged periods in culture, or an exogenous trigger, such as exposure to  
424 oxidative stress or neurotoxins, or excitation-induced calcium influx (Koch et al., 2011).

425 The role of transcriptional dysregulation in the polyQ diseases has been extensively documented,  
426 particularly in cell and animal models of SCA7 (Abou-Sleymane et al., 2006, Chou et al., 2010, Yoo

427 et al., 2003, Tsai et al., 2005, Zijlstra et al., 2010, La Spada et al., 2001). The identification of gene  
428 expression changes, which precede the onset of symptoms, suggests strongly that alterations in  
429 transcription may be among the earliest manifestations of disease (Helmlinger et al., 2006b). Thus, it  
430 follows that gene expression changes may be used as a tool to identify a disease-associated phenotype  
431 in cells representing early stages of development (Feyeux et al., 2012).

432 In order to investigate gene expression changes in the SCA7 iPSCs and iPSC-derived neurons  
433 generated here, a panel of candidate transcripts were selected, in which robust changes had been  
434 previously demonstrated (Palhan et al., 2005, Chou et al., 2010, Tsai et al., 2005, Sopher et al., 2011,  
435 Wang et al., 2010, Luthi-Carter et al., 2002). iPSC-derived neurons and retinal photoreceptors  
436 displayed changes in expression of these key transcripts, suggesting that these cells may serve as useful  
437 models of neurodegenerative disease progression and for the testing of potential therapies (**Figure 6**).

438 Of the three genes consistently downregulated across both differentiated cell types, two (*ATXN7* and  
439 *KAT2A*) encode components of the STAGA transcriptional co-activator complex. Previous studies in  
440 SCA7 patient fibroblasts and mouse models have demonstrated a disease-associated increase in *ATXN7*  
441 expression, mediated by non-coding RNAs (Tan et al., 2014, Sopher et al., 2011). The contradictory  
442 decrease in *ATXN7* expression in SCA7 NPCs and photoreceptors observed here could reflect the early  
443 developmental stage of the cells, but further analysis of the regulatory pathways will be required in  
444 order to elucidate the basis for this apparent decrease in the disease-causing protein in affected cell  
445 types. *KAT2A* encodes the histone acetyltransferase GCN5. Although there are no established links  
446 between *ATXN7* and the expression of *KAT2A*, numerous studies have identified a functional  
447 interaction between the two proteins, which results in changes in STAGA activity in *in vitro* and *in*  
448 *vivo* models of SCA7 (Palhan et al., 2005, Helmlinger et al., 2006a, Chen et al., 2011, Lan et al., 2015,  
449 Paulsen et al., 2017). Loss of GCN5 expression has been shown to result in increased retinal  
450 degeneration in SCA7 mice (Chen et al., 2011).

451 The interaction between *ATXN7* and *CRX* has been hypothesised to be a key factor behind the  
452 development of retinal degeneration in SCA7 patients (La Spada et al., 2001). Therefore the expression  
453 of multiple known *CRX* targets, which were previously shown to be down-regulated in SCA7 mice,  
454 were included in the gene expression experiments. None of these target genes (including *ARR3*,  
455 *GNAT1* or *RHO*) showed consistent changes in patient cells. However, transcriptional changes in the  
456 expression of additional retinal genes, including *OTX2* (involved in the determination of photoreceptor  
457 cell fate), *RCVRN* (expressed in photoreceptors), and *RPE65* (expressed in retinal pigment epithelial  
458 cells), were noted in the patient derived cells. A significant degree of heterogeneity was observed in  
459 the differentiated retinal cells, both in terms of morphology, and gene/protein expression (**Figure 5**),  
460 therefore additional investigation will be required to determine whether these differences can be  
461 attributed to experimental differences or pathogenic mechanisms.

462 Downregulation of the HSP genes *HSP70* and *DNAJ1* was observed in SCA7 patient NPCs. A  
463 decrease in levels of these two HSPs has been previously reported in both SCA7 mice, and human  
464 patient lymphoblasts (Chou et al., 2010, Tsai et al., 2005). Although this decrease in expression was  
465 hypothesised in mice to represent an advanced stage of disease progression, the early developmental  
466 stage recapitulated by our model suggests that decreases in certain HSP genes may instead be an  
467 inherent defect, which could predispose certain populations of cells to degeneration.

468 The generation of patient-specific, disease-relevant cell types is particularly important in  
469 neurodegenerative diseases; as such cells provide a unique model in which to evaluate disease  
470 pathogenesis without the complications associated with transgene overexpression in cell or animal

471 models. In addition, the use of cells containing the patient's own genetic background offers the  
472 opportunity to investigate potential modifiers of disease onset and progression (Marsh and Thompson,  
473 2006; Bilen and Bonini, 2007,). Perhaps most importantly to the South African context, iPSC-derived  
474 neurons provide the first opportunity to evaluate the efficacy of the allele-specific RNAi-based therapy  
475 developed by Scholefield et al. (2009), in disease-affected cells.

476 One significant caveat of this study remains the small number of patients assessed – a consequence of  
477 the rare nature of the condition, and the challenges associated with patient recruitment in a developing  
478 world setting, in which many of those affected are unable to access tertiary healthcare. Future studies  
479 will focus on recruitment, in order to extend these investigations in a larger patient cohort. To control  
480 for the inherent genetic variability associated with comparisons between unrelated patients, future work  
481 will also focus on the generation of isogenic control lines, by means of CRISPR/Cas9-mediated  
482 genome editing.

483 Nevertheless, the SCA7 iPSCs generated here serve as a resource for differentiation into a variety of  
484 disease-associated cell types, providing an ideal model in which to study neurodegenerative diseases.  
485 The results of this study provide the first evidence of a disease phenotype in iPSC-derived cells from  
486 the South African SCA7 patient cohort, paving the way for future analysis of pathogenesis, and the  
487 development of population-specific therapies.

## 488 5. Abbreviations

489 CRX, cone-rod homebox; iPSC, induced pluripotent stem cells; NPC, neuronal progenitor cells; PCR,  
490 polymerase chain reaction; polyQ, polyglutamine; SCA7, spinocerebellar ataxia type 7; SeVdp, Sendai  
491 virus vectors; STAGA; SPT3-TAF9-ADA-GCN5 acetyltransferase.

## 492 493 6. Supporting Information

494 **Figure S-1.1** shows a representative karyogram of an iPSC line, showing no gross structural  
495 abnormalities. **Figure S-1.2** shows how iPSCs, retinal cells and NPCs were differentiated by semi-  
496 quantitative PCR. **Figure S-1.3** shows transcriptional changes in SCA7 patient-derived fibroblasts,  
497 compared to unaffected control fibroblasts.

498 Summary of SCA7 patient and unaffected control cell lines, genotypes and ages is shown in **Table S-**  
499 **1.1**. The various antibodies for immunocytochemistry used are summarised in **Table S-1.2** while the  
500 primer sequences used are shown in **Table S-1.3**.

## 501 7. Conflict of Interests

502 The authors declare that the research was conducted in the absence of any commercial or financial  
503 relationships that could be construed as a potential conflict of interest.

## 504 8. Author Contributions

505 **LMW**, iPSC culture experimental work for neuronal cells, molecular studies, imaging, writing of  
506 manuscript; **DCS**, iPSC culture experimental work for retinal cells, imaging, molecular studies, writing  
507 of manuscript; **JVR**, electrophysiology experimental work, data analysis thereof, writing of  
508 manuscript; **RJB**, electrophysiology experimental work, data analysis thereof, writing of manuscript;  
509 **RB**, iPSC generation; **JS**, technical supervision for iPSC culture and imaging; **SAC**, supervision of  
510 iPSC culture and molecular experiments; **MJAW**, supervision of molecular studies; **SHK**, supervision



511 of iPSC differentiation, assisted in writing of manuscript; **LJG**, principle investigator, patient  
512 recruitment, supervision of iPSC culture and molecular studies and assisted in writing of manuscript.

## 513 **9. Funding**

514 Funding for this work was provided by Ataxia UK, Commonwealth Scholarship Commission (UK),  
515 John Fell OUP Fund, National Research Foundation (South Africa), National Research Foundation  
516 (South Africa, Competitive Programme for Rated Researchers CPR20110624000019696), Medical  
517 Research Council (South Africa), Harry Crossley Foundation, Deutscher Akademischer Austausch  
518 Dienst, University of Cape Town Research Council, Wellcome Trust, Parkinson's Disease UK,  
519 Medical Research Council UK, Blue Brain Project, and the James Martin 21<sup>st</sup> Century School.  
520 Electrophysiology equipment was provided by the École Polytechnique Fédérale de Lausanne,  
521 Switzerland.

## 522 **10. Acknowledgements**

523 The authors thank Dr Mahito Nakanishi for kind provision of the Sendai virus vector, Ms Jane Vowles  
524 for assistance with iPSC generation, and Ms Theresa Ruppelt and colleagues at the South African  
525 National Health Laboratory Service for karyotype analyses. We honour the late Ms Ingrid Baumgarten  
526 for her invaluable assistance over many years, particularly in establishing patient fibroblast cultures.

## 527 **11. References**

- 528 Abou-Sleymane G, Chalmel F, Helminger D, Lardenois A, Thibault C, Weber C, et al. Polyglutamine  
529 expansion causes neurodegeneration by altering the neuronal differentiation program. *Human*  
530 *Molecular Genetics* (2006) 15: 691-703. doi: 10.1093/hmg/ddi483s.
- 531 Ansorge O, Giunti P, Michalik A, Van Broeckhoven C, Harding B, Wood N, et al. Ataxin-7  
532 aggregation and ubiquitination in infantile SCA7 with 180 CAG repeats. *Annals of Neurology* (2004)  
533 56: 448-452. doi: 10.1002/ana.20230.
- 534 Arrasate M, Mitra S., Schweitzer ES, Segal MR & Finkbeiner S Inclusion body formation reduces  
535 levels of mutant huntingtin and the risk of neuronal death. *Nature* (2004) 431: 805-810. doi:  
536 10.1038/nature02998.
- 537 Belinsky GS, Moore AR, Short SM, Rich MT & Antic SD. Physiological properties of neurons derived  
538 from human embryonic stem cells using a dibutyryl cyclic AMP-based protocol. *Stem Cells*  
539 *Development* (2011) 20:1733-1746. doi: 10.1089/scd.2010.0501.
- 540 Belinsky GS, Rich MT, Sirois CL, Short SM, Pedrose E, Lachman HM & Antic SD. Patch-clamp  
541 recordings and calcium imaging followed by single-cell PCR reveal the developmental profile of 13  
542 genes in iPSC-derived human neurons. *Stem Cell Research* (2014) 12: 101-118. doi:  
543 10.1089/scd.2010.0501.
- 544 Boucherie C, Mukherjee S, Henckaerts E, Thrasher AJ, Sowden JC and Ali RR. Brief report: Self-  
545 organizing neuroepithelium from human pluripotent stem cells facilitates derivation of  
546 photoreceptors. *Stem cells* (2013) 31:408-414. doi: 10.1002/stem.1268.
- 547 Bilen J & Bonini NM. Genome-wide screen for modifiers of ataxin-3 neurodegeneration in *Drosophila*.  
548 *PLoS Genetics* (2007) 3: e177. doi: 10.1371/journal.pgen.0030177.
- 549 Bustin SA, Benes V, Garson JA, Hellemans J, Huggett J, Kubista M, et al. The MIQE guidelines:  
550 minimum information for publication of quantitative real-time PCR experiments. *Clinical chemistry*  
551 (2009) 55: 611-622. doi: 10.1111/eci.12801

- 552 Camnasio S, Carri AD, Lombardo A, Grad I, Mariotti C, Ca stucci A, Rozell B, Riso PL, Castiglioni  
553 V & Zuccato C. The first reported generation of several induced pluripotent stem cell lines from  
554 homozygous and heterozygous Huntington's disease patients demonstrates mutation related enhanced  
555 lysosomal activity. *Neurobiology of Disease* (2012) 46: 41-51. doi: 10.1016/j.nbd.2011.12.042.
- 556 Chen TC, Gatchel JR, Lewis RW, Mao CA, Grant PA, Zoghbi HY, et al. Gcn5 loss-of-function  
557 accelerates cerebellar and retinal degeneration in a SCA7 mouse model. *Human Molecular Genetics*  
558 (2011) 21: 394-405. doi: 10.1093/hmg/ddr474.
- 559 Chou AH, Chen CY, Chen SY, Chen Wj, Chen YL, Weng YS, et al. Polyglutamine-expanded ataxin-  
560 7 causes cerebellar dysfunction by inducing transcriptional dysregulation. *Neurochemistry*  
561 *International* (2010) 56: 329-339. doi: 10.1016/j.neuint.2009.11.003.
- 562 Duvick L, Barnes J, Ebner B, Agrawal S, Andresen M, Lim J, et al. SCA1-like disease in mice  
563 expressing wild-type ataxin-1 with a serine to aspartic acid replacement at residue 776. *Neuron* (2010)  
564 67 929-935. doi: 10.1016/j.neuron.2010.08.022.
- 565 Einum DD, Townsend JJ, Ptacek LJ & FU YH. Ataxin-7 expression analysis in controls and  
566 spinocerebellar ataxia type 7 patients. *Neurogenetics* (2001) 3: 83-90.
- 567 Feyeux M, Bougois-Rocha F, Redfern A, Giles P, LeFort N, Aubert S, et al. Early transcriptional  
568 changes linked to naturally occurring Huntington's disease mutations in neural derivatives of human  
569 embryonic stem cells. *Human Molecular Genetics* (2012) 21: 3883-3895. doi: 10.1093/hmg/dds216.
- 570 Frechney RI. Specialized cells. *Culture of Animal Cells: A Manual of Basic Technique and Specialized*  
571 *Applications*. New Jersey: Wiley-Blackwell (2000). 383-432.
- 572 Garden GA & La Spada. Molecular pathogenesis and cellular pathology of spinocerebellar ataxia type  
573 7 neurodegeneration. *The Cerebellum* (2008) 7: 138-149.
- 574 Garden GA, Libby RT, Fu YH, Kinoshita Y, Huang J, Possin DE et al. Polyglutamine-expanded ataxin-  
575 7 promotes non-cell-autonomous purkinje cell degeneration and displays proteolytic cleavage in ataxic  
576 transgenic mice. *Journal of Neuroscience* (2012) 22: 4897-4905.
- 577 Gouw L, Digre K, Harris C, Haines J & Ptacek :OUW, L., DIGRE, K., HARRIS, C., HAINES, J. &  
578 PTACEK, L. Autosomal dominant cerebellar ataxia with retinal degeneration Clinical,  
579 neuropathologic, and genetic analysis of a large kindred. *Neurology*, (1994) 44: 1441-1441. doi:  
580 10.1111/j.1399-0004.2006.00680.
- 581 Greenberg J, Solomon G, Vorster A, Heckmann J & Bryer A. Origin of the SCA7 gene mutation in  
582 South Africa: implications for molecular diagnostics. *Clinical genetics* (2006) 70: 415-417. doi:  
583 10.1111/j.1399-0004.2006.00680.
- 584 Handsen ST, Meera P, Otis TS & Pulst SM. Changes in Purkinje cell firing and gene expression  
585 precede behavioral pathology in a mouse model of SCA2. *Human Molecular Genetics* (2012) 22: 271-  
586 283. doi:10.1093/hmg/dds427.
- 587 Hartl FU, Bracher A & Hayer-Hartl M. Molecular chaperones in protein folding and proteostasis.  
588 *Nature* (2011) 475: 324. doi: 10.1038/nature10317.
- 589 Helminger D, Hardy S, Eberlin A, Devys D & Tora L. Both normal and polyglutamine-expanded  
590 ataxin-7 are components of TFTC-type GCN5 histone acetyltransferase-containing complexes.  
591 *Biochemical Society Symposia*, 2006a. London; Portland on behalf of The Biochemical Society;  
592 (1999) 155.
- 593 Helminger D, Tora L & Devys D. Transcriptional alterations and chromatin remodeling in  
594 polyglutamine diseases. *Trends in Genetics* (2006) 22: 562-570.

- 595 Jonasson J, Strom AL, Hart P, Brannstrom T, Forsgren L & Holmberg M. Expression of ataxin-7 in  
596 CNS and non-CNS tissue of normal and SCA7 individuals. *Acta Neuropathologica* (2002) 104: 29-37.  
597 doi: 10.1007/s00401-001-0514-4.
- 598 Koch P, Breuer P, Peitz M, Jungverdorben J, Kesavan J, Poppe D, et al. Excitation-induced ataxin-3  
599 aggregation in neurons from patients with Machado–Joseph disease. *Nature* (2011) 480: 543. doi:  
600 10.1038/nature10671.
- 601 Larionov A, Krause A and Miller W. A standard curve based method for relative real time PCR data  
602 processing. *BMC bioinformatics* (2005) 6: 62-77. [10.1186/1471-2105-6-62](https://doi.org/10.1186/1471-2105-6-62)
- 603 La Spada AR, Fu YH, Sopher BL, Libby RT, Wang X, Li LY, et al. Polyglutamine-expanded ataxin-  
604 7 antagonizes CRX function and induces cone-rod dystrophy in a mouse model of SCA7. *Neuron*  
605 (2001) 31: 913-927.
- 606 Li W, Sun W, Zhang Y, Wei W, Ambasudhan R, Xia P, Talantova M, et al. Rapid induction and long-  
607 term self-renewal of primitive neural precursors from human embryonic stem cells by small molecule  
608 inhibitors. *Proceedings of the National Academy of Sciences* (2011) 108: 8299-8304.
- 609 Luo Y, Fan Y, Zhou B, Xu Z, Chen Y & Sun X. Generation of induced pluripotent stem cells from  
610 skin fibroblasts of a patient with olivopontocerebellar atrophy. *The Tohoku Journal of Experimental*  
611 *Medicine* (2012) 226: 151-159.
- 612 Luthi-Carter R, Strand AD, Hanson SA, Kooperberg C, Schilling G, La Spada AR, et al. Polyglutamine  
613 and transcription: gene expression changes shared by DRPLA and Huntington's disease mouse models  
614 reveal context-independent effects. *Human Molecular Genetics* (2002) 11, 1927-1937.
- 615 March JL & Thompson LM. *Drosophila* in the study of neurodegenerative disease. *Neuron* (2006) 52:  
616 169-178. doi: 10.1016/j.neuron.2006.09.025.
- 617 Martl M, Mulero L, Pardo C, Morera C, Carrio M, Laricchia-Robbio, et al. Characterization of  
618 pluripotent stem cells. *Nature Protocols* (2013) 8: 223. doi: 10.1038/nprot.2012.154.
- 619 Miller J, Arrasate M, Shaby BA, Mitra S, Masliah E & Finkbeiner S. Quantitative relationships  
620 between huntingtin levels, polyglutamine length, inclusion body formation, and neuronal death provide  
621 novel insight into huntington's disease molecular pathogenesis. *Journal of Neuroscience* (2010) 30:  
622 10541-10550. doi: 10.1523/JNEUROSCI.0146-10.2010.
- 623 Monckton DG, Cayuela ML, Gould FK, Brock GJ, de Silva R & Ashizawa T. Very large (CAG) n  
624 DNA repeat expansions in the sperm of two spinocerebellar ataxia type 7 males. *Human Molecular*  
625 *Genetics* (1999) 8: 2473-2478.
- 626 Moody & Bosma MM. Ion channel development, spontaneous activity, and activity-dependent  
627 development in nerve and muscle cells. *Physiological Reviews* (2005) 85: 883-941. doi:  
628 10.1152/physrev.00017.2004.
- 629 Moore AR, Filipovic R, Mo Z, Rasband MN, Zecevic N & Antic SD. Electrical excitability of early  
630 neurons in the human cerebral cortex during the second trimester of gestation. *Cerebral Cortex* (2009)  
631 19:1795-1805. doi: 10.1093/cercor/bhn206.
- 632 Muguruma, K. Self-Organized Cerebellar Tissue from human pluripotent stem cells and disease  
633 modeling with patient-derived iPSCs. *The Cerebellum* (2017) 1597: 1-5. doi: 10.1007/978-1-4939-  
634 6949-4\_3.
- 635 Nakanishi M & Otsu M. Development of Sendai virus vectors and their potential applications in gene  
636 therapy and regenerative medicine. *Current Gene Therapy* (2012) 12: 410-416.

- 637 Nishimura K, Sano M, Phtaka M, Furuta B, Imemura Y, Nakajima Y, et al. Development of defective  
638 and persistent Sendai virus vector a unique gene delivery/expression system ideal for cell  
639 reprogramming. *Journal of Biological Chemistry* (2011) 286: 4760-4771. doi:  
640 10.1074/jbc.M110.183780.
- 641 Orr HT & Zoghbi HY Trinucleotide repeat disorders. *Annuals Reviews Neuroscience* (2007) 30: 575-  
642 621. doi: 10.1146/annurev.neuro.29.051605.113042.
- 643 Palhan VB, Chen S, Peng GH, Tjernberg A, Gamper AM, Fan Y, et al. Polyglutamine-expanded ataxin-  
644 7 inhibits STAGA histone acetyltransferase activity to produce retinal degeneration. *Proceedings of*  
645 *the National Academy of Sciences of the United States of America* (2005) 102: 8472-8477. doi:  
646 10.1073/pnas.0503505102.
- 647 Paulson HL, Shakkottai VG, Clark HB and Orr HT. Polyglutamine spinocerebellar ataxias—from  
648 genes to potential treatments. *Nature Reviews Neuroscience* (2017) 18: 613 - 626. doi:  
649 10.1038/nrn.2017.92.
- 650 Perrier AL, Tabar V, Barberi T, Rubio ME, Bruses J, Topf N, et al. Derivation of midbrain dopamine  
651 neurons from human embryonic stem cells. *Proceedings National Academy Science U S A* (2004)  
652 101:12543-12548. doi: 10.1073/pnas.0404700101.
- 653 Scholefield J, Greenberg LJ, Weinberg MS, Arbuthnot PB, Abdelgany A & Wood MJ. Design of RNAi  
654 hairpins for mutation-specific silencing of ataxin-7 and correction of a SCA7 phenotype. *PloS One*  
655 (2009) 4: e7232. doi: 10.1371/journal.pone.0007232.
- 656 Scholefield J, Watson L, Smith D, Greenberg J & Wood MJ. Allele-specific silencing of mutant  
657 Ataxin-7 in SCA7 patient-derived fibroblasts. *European Journal of Human Genetics* (2014) 22: 1369.  
658 doi: 10.1038/ejhg.2014.39.
- 659 Smith D, Bryer A, Watson L & Greenberg LJ. Inherited polyglutamine spinocerebellar ataxias in South  
660 Africa. *South African Medical Journal* (2012) 102: 683-686. doi: 10.1016/j.jns.2015.04.053.
- 661 Smith DC, Atadzhanov M, Mwaba M & Greenberg LJ. Evidence for a common founder effect amongst  
662 South African and Zambian individuals with Spinocerebellar ataxia type 7. *Journal of the Neurological*  
663 *Sciences* (2015) 354: 75-78. doi: 10.1016/j.jns.2015.04.053.
- 664 Soldner F, Hockemeyer D, Beard C, Gao Q, Bell GW, Cook EG, et al. Parkinson's disease patient-  
665 derived induced pluripotent stem cells free of viral reprogramming factors. *Cell* (2009) 136: 964-977.  
666 doi: 10.1016/j.cell.2009.02.013.
- 667 Sopher BL, Ladd, PD, Pineda VV, Libby RT, Sunkin SM, Hurley JB, et al. CTCF regulates ataxin-7  
668 expression through promotion of a convergently transcribed, antisense noncoding RNA. *Neuron* (2007)  
669 70: 1071-1084. doi: 10.1016/j.neuron.2011.05.027.
- 670 Strom AL, Forsgren L & Homberg M. A role for both wild-type and expanded ataxin-7 in  
671 transcriptional regulation. *Neurobiology of Disease* (2005) 20: 646-655. doi:  
672 10.1016/j.nbd.2005.04.018.
- 673 Takahashi K, Tanabe K, Ohnuki M, Narita M, Ichisaka T, Tomoda K & Yamanaka S. Induction of  
674 pluripotent stem cells from adult human fibroblasts by defined factors. *Cell* (2007) 131: 861-872. doi:  
675 10.1016/j.cell.2007.11.019.
- 676 Takahashi K, Yamanaka S. Induction of pluripotent stem cells from mouse embryonic and adult  
677 fibroblast cultures by defined factors. *Cell* (2006) 126: 663-676. doi: 10.1016/j.cell.2006.07.024.

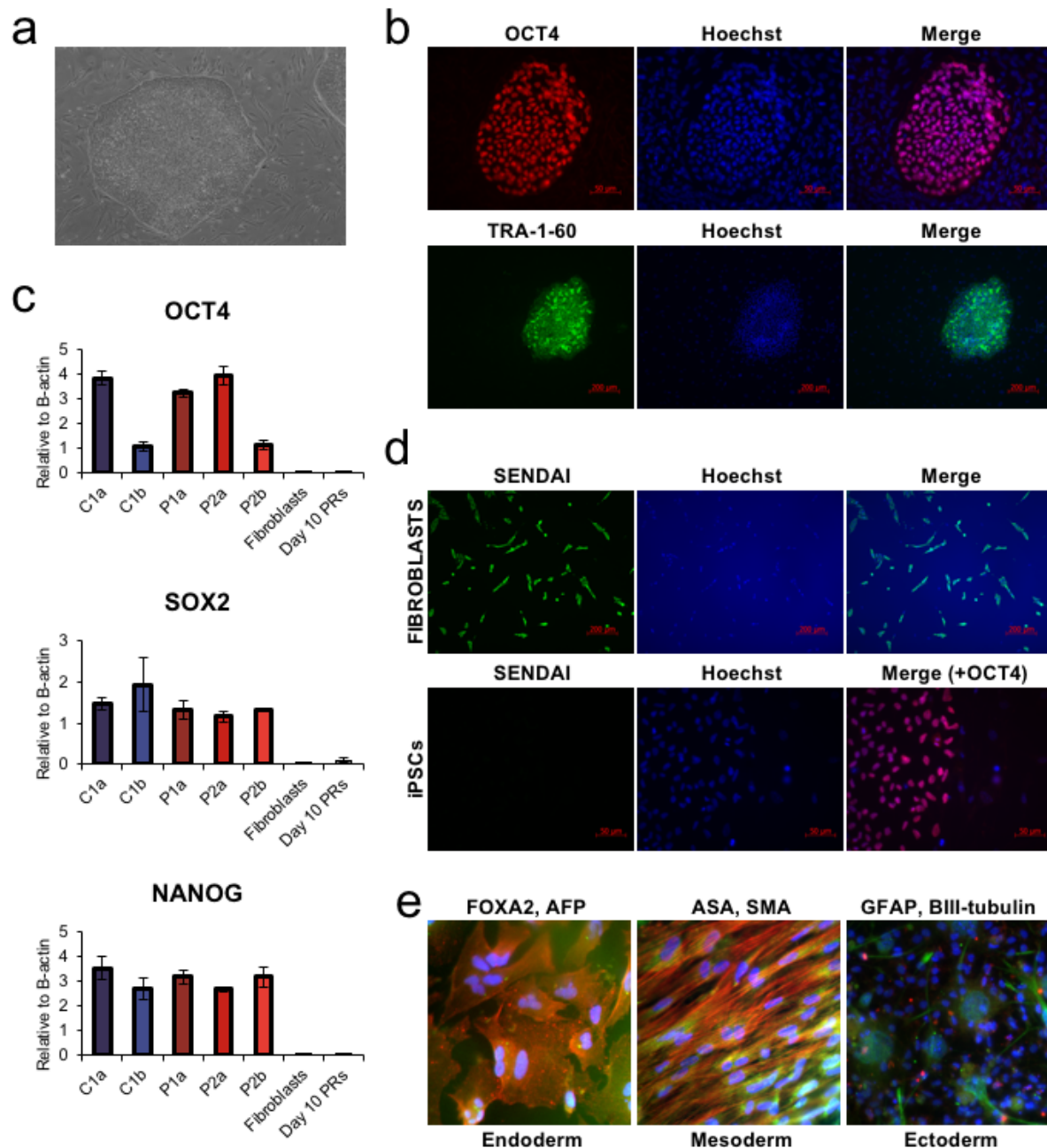


- 678 Tan JY, Vance KW, Varela MA, Sirey T, Watson LM, Curtis HJ, et al. Cross-talking noncoding RNAs  
679 contribute to cell-specific neurodegeneration in SCA7. *Nature Structural and Molecular Biology*  
680 (2014) 21: 955. doi: 10.1038/nsmb0315-272b.
- 681 Taylor J, Grote SK, Xia J, Vandelft M, Graczyk J, Ellerby LM, et al. Ataxin-7 can export from the  
682 nucleus via a conserved exportin-dependent signal. *Journal of Biological Chemistry* (2006) 281: 2730-  
683 2739. doi: 10.1074/jbc.M506751200.
- 684 Todd TW & Lim J Aggregation formation in the polyglutamine diseases: protection at a cost?  
685 *Molecules and Cells* (2013) 36: 185-194. doi: 10.1007/s10059-013-0167-x.
- 686 Tsai HF, Lin SJ, Li C & Hsieh M. Decreased expression of Hsp27 and Hsp70 in transformed  
687 lymphoblastoid cells from patients with spinocerebellar ataxia type 7. *Biochemical and biophysical*  
688 *research communications* (2005) 334: 1279-1286.
- 689 Wang HL, Chou AH, Lin AC, Chen SY, Weng YH & Yeh THANG, H.-L Polyglutamine-expanded  
690 ataxin-7 upregulates Bax expression by activating p53 in cerebellar and inferior olivary neurons.  
691 *Experimental Neurology* (2010) 224: 486-494. doi: 10.1016/j.expneurol.2010.05.011.
- 692 Watson LM, Wong MM & Becker EB. Induced pluripotent stem cell technology for modelling and  
693 therapy of cerebellar ataxia. *Open Biology* (2015) 5: 150056. doi: 10.1098/rsob.150056.
- 694 Watson LM, Wong MM, Vowles J, Cowley SA and Becker EB. A Simplified Method for Generating  
695 Purkinje Cells from Human-Induced Pluripotent Stem Cells. *The Cerebellum* (2018): 1-9. doi:  
696 10.1007/s12311-017-0913-2.
- 697 Watson LM, Wood MJA, Smith DC, Scholefield J, Ballo R, Kidson S and Greenberg LJ.  
698 Spinocerebellar ataxia type 7 in South Africa: epidemiology, pathogenesis and therapy: the new  
699 millennium. *South African Medical Journal* (2016) 106: 107-109. doi:  
700 10.7196/SAMJ.2016.v106i6.11010.
- 701 Yoo SY, Pennesi ME, Weeber EJ, Xu B, Atkinson R, Chen S, et al. SCA7 knockin mice model human  
702 SCA7 and reveal gradual accumulation of mutant ataxin-7 in neurons and abnormalities in short-term  
703 plasticity. *Neuron* (2003) 37: 383-401.
- 704 Young JE, Gouw L, Propp S, Sopher BL, Taylor J, Lin A, et al. Proteolytic cleavage of ataxin-7 by  
705 caspase-7 modulates cellular toxicity and transcriptional dysregulation. *Journal of Biological*  
706 *Chemistry* (2007) 282: 30150-30160. doi: 10.1074/jbc.M705265200.
- 707 Zijlstra M, Rujano M, Van Waarde M, Vis E, Brunt E & Kampinga H. Levels of DNAJB family  
708 members (HSP40) correlate with disease onset in patients with spinocerebellar ataxia type 3. *European*  
709 *Journal of Neuroscience* (2010) 32: 760-770. doi: 10.1111/j.1460-9568.2010.07352.x.

710

711

712 **12. Figures**

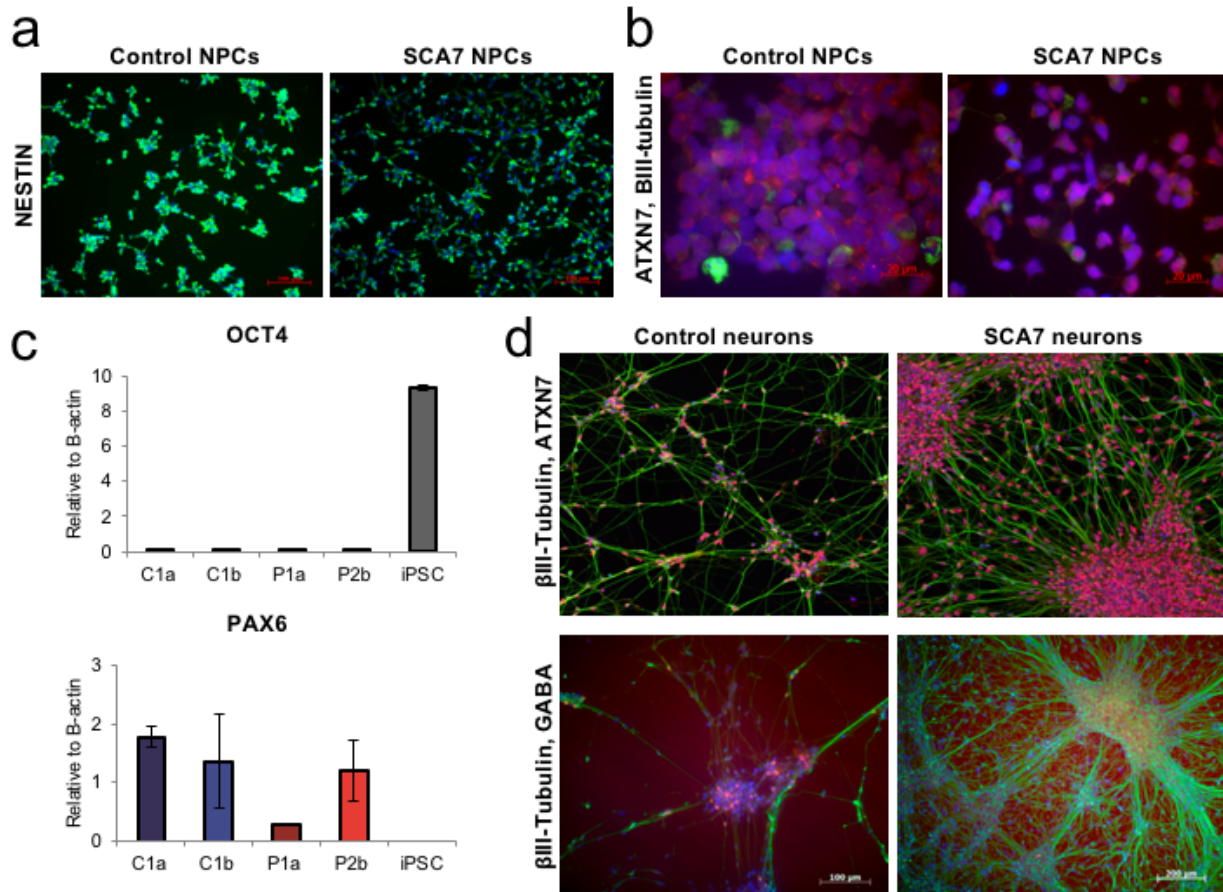


713

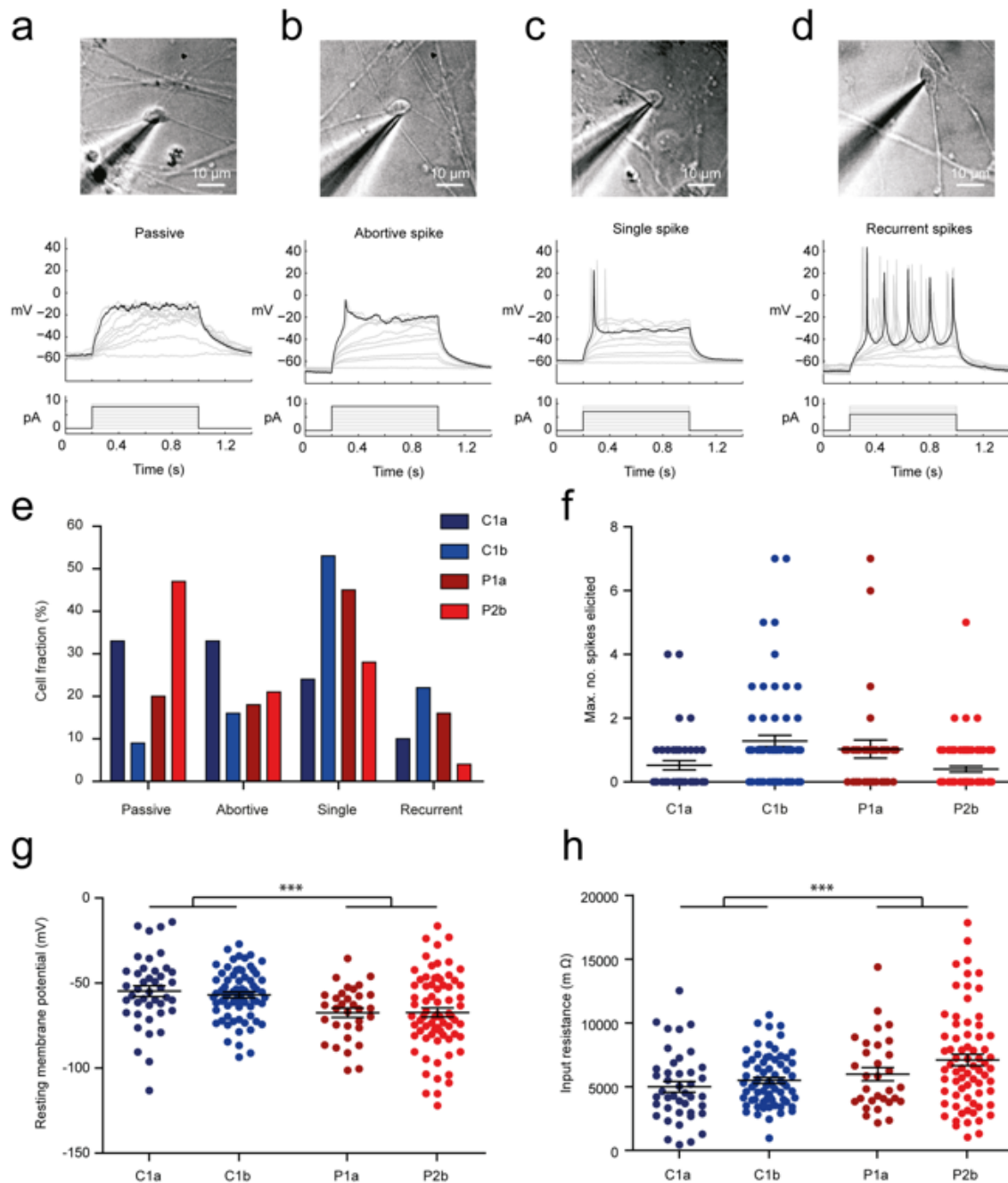
714

715 **Figure 1:** iPSC characterisation. **a)** Morphology of iPSC colonies. Colonies could be seen as groups  
 716 of tightly packed cells with a high nuclear-to-cytoplasm ratio. **b)** Representative immunocytochemistry  
 717 image showing positive OCT4 staining (red, top panel) and TRA-1-60 staining (green, bottom panel)  
 718 in iPSCs. **c)** Expression of pluripotency markers in iPSC lines, determined by qPCR. All five iPSC  
 719 lines (P1a, P2a, P2b, C1a, C1b) expressed OCT4, SOX2 and NANOG, compared to low expression  
 720 levels in the original donor fibroblasts, or cells subjected to the retinal differentiation protocol for 10  
 721 days (pooled data from lines P2b and C1b). All levels shown relative to beta actin (ACTB). **d)**  
 722 Immunocytochemistry in newly infected fibroblasts (top panel) and iPSC colonies (bottom panel)  
 723 co-stained with primary antibodies against OCT4 (red) and the viral nucleocapsid protein (green) showed  
 724 effective silencing of the reprogramming Sendai virus. **e)** The five iPSC lines (P1a, P2a, P2b, C1a,

725 C1b) were subjected to differentiation protocols to produce cells from either the endodermal,  
726 mesodermal or ectodermal lineages. Endodermal cells stained positive for either Forkhead box A2  
727 (FOXA2, green) or Alpha-fetoprotein (AFP, red). Mesodermal cells expressed either Sarcomeric alpha  
728 actinin (ASA, green) or Smooth muscle actin (SMA, red). Ectodermal cells expressed Glial fibrillary  
729 acidic protein (GFAP, red) or  $\beta$ III-tubulin (green).  
730



731  
732  
733 **Figure 2:** Characterisation of iPSC-derived NPCs. **a)** Representative images of control (left panel)  
734 and SCA7 patient (right panel) NPCs, expressing the early neural marker, Nestin (green). **b)** High  
735 magnification images showing nuclear expression of ATXN7 (red) in control (left) and patient (right)  
736 NPCs (Green:  $\beta$ III-Tubulin). **c)** qPCR results indicating suppression of *OCT4* and upregulation of  
737 *PAX6* expression in NPCs, compared with the iPSC lines from which they were derived. All levels  
738 shown relative to beta actin (ACTB). **d)** Control (left) and SCA7 (right) NPC-derived neurons stain  
739 positive for  $\beta$ III-Tubulin (green) and ATXN7 (red) after 14 days of differentiation (top panel). Both  
740 control (left) and SCA7 patient (right) NPCs produced a small proportion of GABA-positive neurons  
741 (red) after 14 days in culture (bottom panel) (Green:  $\beta$ III-Tubulin).  
742  
743  
744  
745  
746

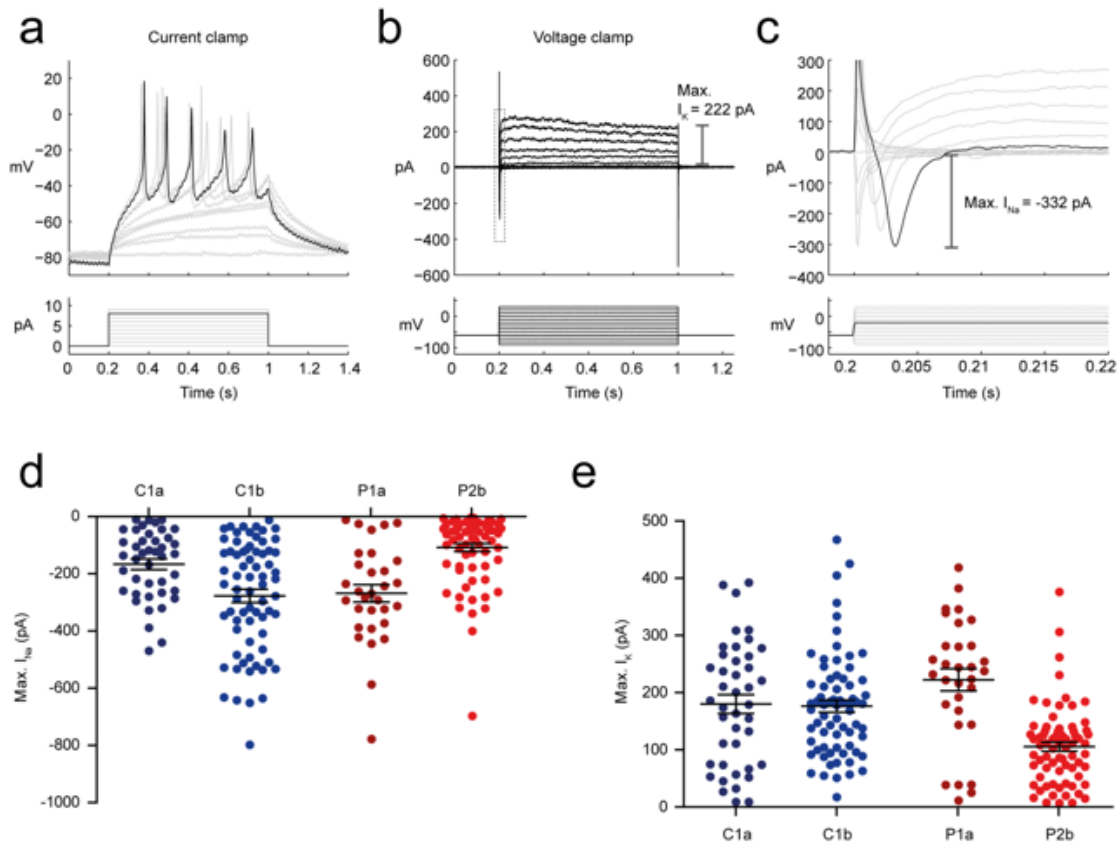


747  
748

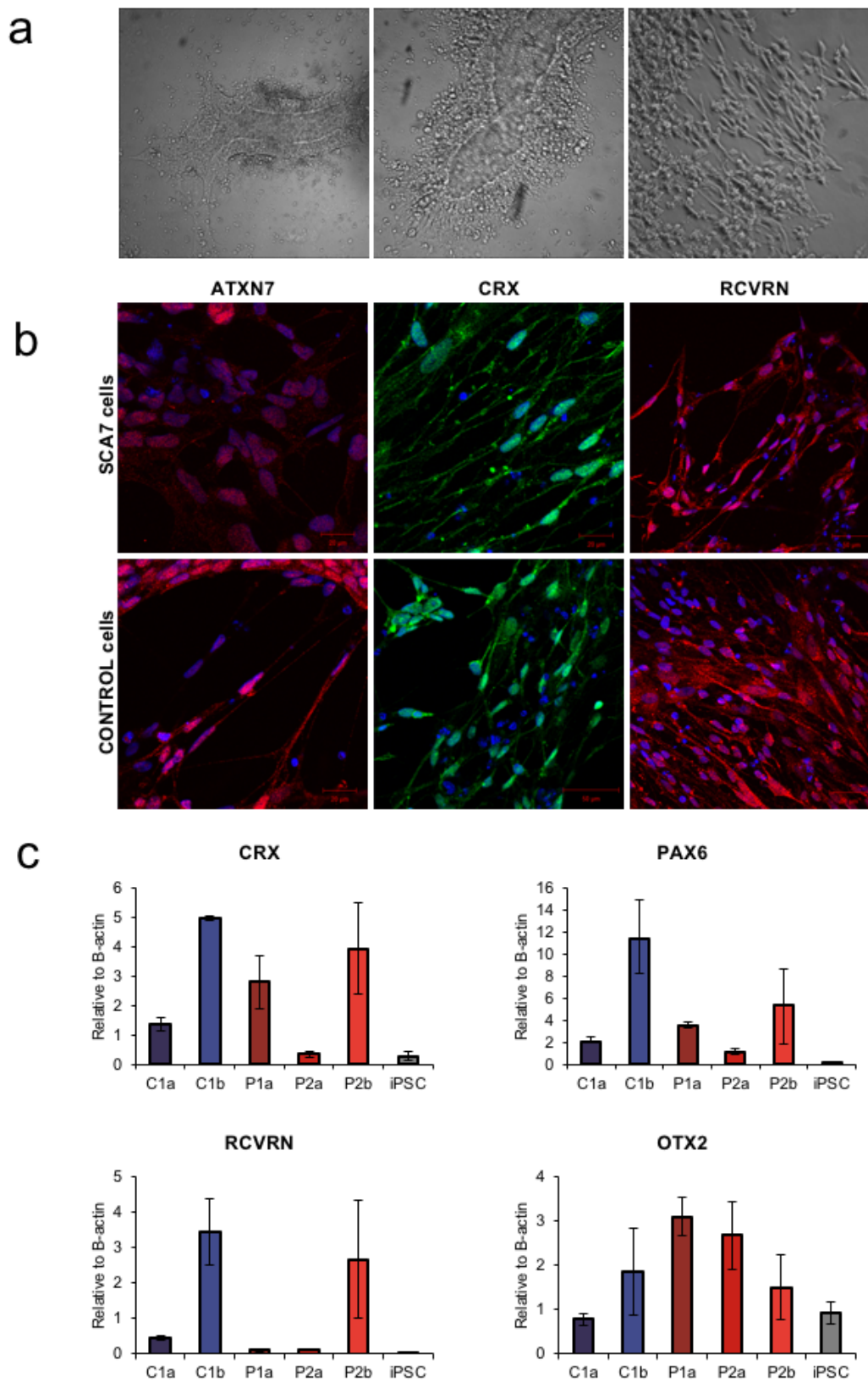
749 **Figure 3:** Patch-clamp analyses of iPSC derived neuronal cultures. Cells could be divided into four  
750 categories based on their spiking responses. a)-d) Differential interference contrast images of cells  
751 targeted for patch-clamp recordings (top). Whole-cell recordings in current clamp mode (middle)  
752 depict spiking patterns following injection of current (bottom). Cells fell into (a) ‘passive’, (b)  
753 ‘abortive spike’, (c) ‘single spike’ and (d) ‘recurrent spikes’ categories. e) The fraction of cells which  
754 fell into each category for cells derived from two control and two SCA7 patient iPSC lines. Note that  
755 although the cells derived from various iPSC lines exhibited different distributions of spiking  
756 responses, no trend between control and patient lines was observed. f) Maximum number of spikes  
757 elicited by current injection for each recorded cell according to the iPSC line. g) The resting membrane  
758 potentials of cells derived from SCA7 patients were significantly more negative than controls. h) Cell



759 input resistance was also significantly increased in SCA7 patient lines as compared to control lines.  
760 Error bars denote mean  $\pm$  SEM, \*\*\*  $p < 0.001$ .  
761



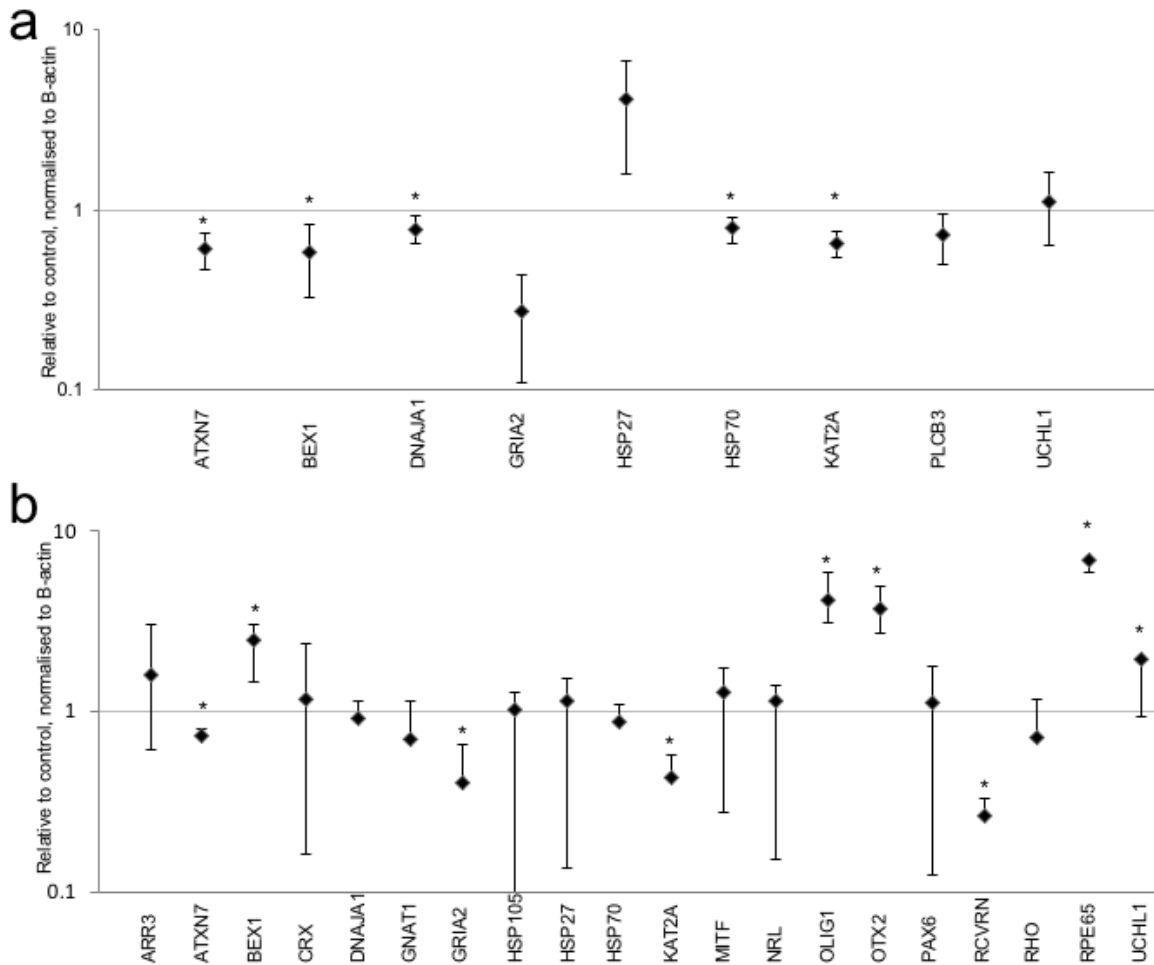
762  
763  
764 **Figure 4:** Sodium and potassium currents in neurons differentiated from control and patient iPS cell  
765 lines. **a)** Current-clamp recording demonstrating recurrent spikes elicited from a cell following current  
766 injection. **b)** Voltage-clamp recording from the same cell in 'a'. Membrane currents (top) were  
767 recorded following 10 mV voltage steps between -90 and 30 mV (bottom). Dashed gray rectangle  
768 indicates the position of voltage-gated sodium currents (enhanced in 'c'). Maximum potassium current  
769 is indicated 'right'. **c)** Zoom-in of rectangle in 'b' with the maximum sodium current highlighted.  
770 Population data from the four iPSC lines for maximum voltage-gated sodium (**d**) and maximum  
771 potassium (**e**) currents respectively. No consistent trend between control and patient lines was  
772 observed. Error bars denote mean  $\pm$  SEM.  
773  
774  
775  
776  
777  
778  
779  
780  
781  
782  
783



784  
785  
786  
787  
788

**Figure 5:** Characterisation of iPSC-derived retinal cells. **a)** Representative bright field images of iPSCs undergoing retinal differentiation on day 2 (first column, 10x magnification), day 4 (middle column, 25x magnification) and day 25 (last column, 20x magnification). **b)** Immunocytochemical analysis of

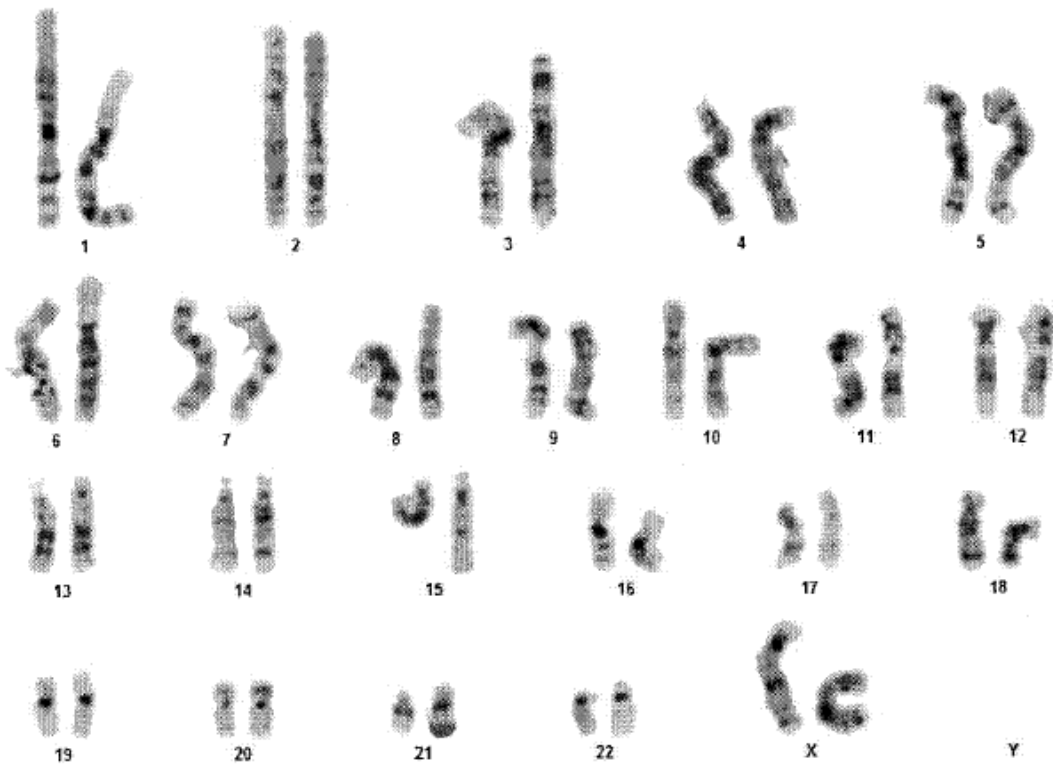
789 SCA7 (top panel) and control (bottom panel) retinal cells showed positive staining for ATXN7  
 790 (ATXN7, first column, red), cone-rod homeobox (CRX, middle column, green) and recoverin  
 791 (RCVRN, last column, red) on day 30 of the differentiation experiment. Nuclei in blue. c) qPCR results  
 792 confirmed the expression of *CRX*, *PAX6*, *RCVRN* and *OTX2* in all five lines, compared with the iPSC  
 793 lines from which they were derived. All levels shown relative to beta actin (ACTB).  
 794



795  
 796  
 797 **Figure 6:** Transcriptional changes in SCA7 iPSC-derived NPCs and retinal cells. **a)** Expression of 9  
 798 selected genes in SCA7 patient NPCs (n = 2) shown relative to unaffected control NPCs (n = 2). **b)**  
 799 Expression of 23 selected genes in SCA7 patient iPSC-derived retinal cells (n=2) shown relative to  
 800 unaffected control cells (n = 1). All levels shown relative to beta actin (ACTB) and unaffected control  
 801 cells. \*\*\*  $p \leq 0.05$ .

802  
 803  
 804  
 805  
 806  
 807  
 808  
 809

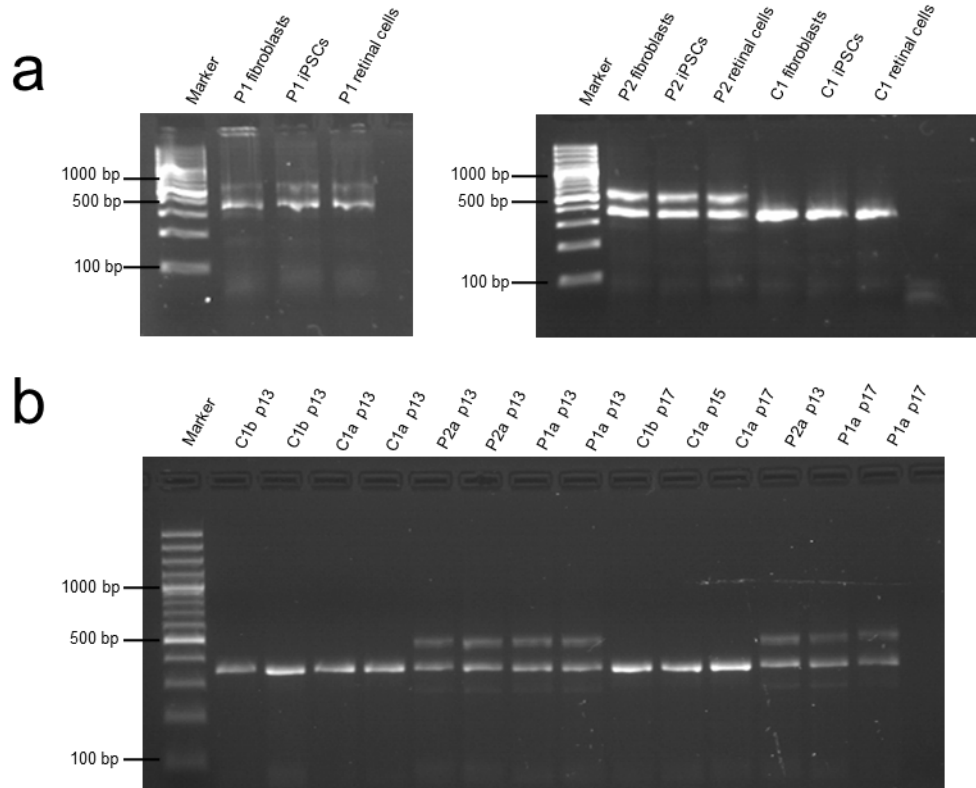
810 **13. Supplementary Material**



811  
812  
813  
814  
815  
816  
817  
818  
819  
820  
821  
822  
823  
824  
825  
826  
827  
828  
829  
830  
831  
832  
833  
834  
835  
836  
837  
838  
839  
840

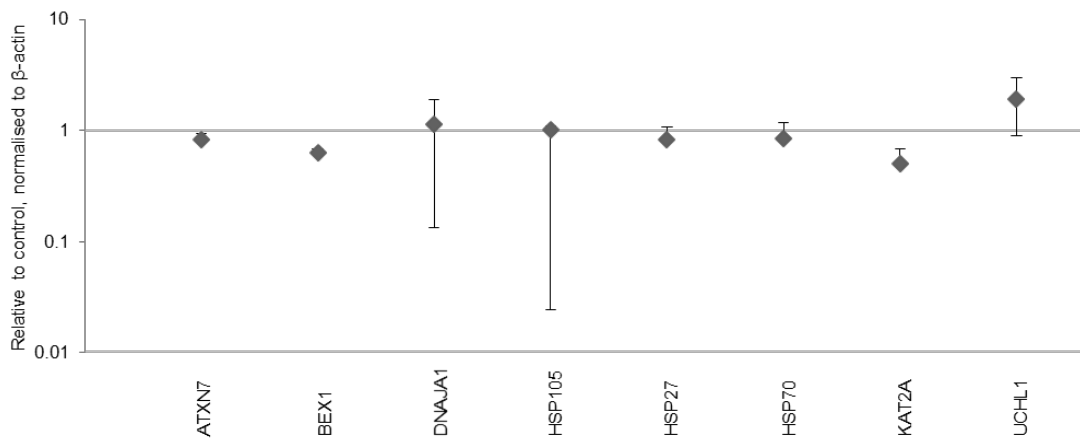
**Figure S-1.1:** Representative karyogram of an iPSC line, showing no gross structural abnormalities





841  
842  
843  
844  
845  
846  
847  
848

**Figure S-1.2** iPSCs, retinal cells (a) and NPCs (b), by semi-quantitative PCR. Samples from all three individuals showed a single band at approximately 355bp, corresponding with a wild-type allele, whilst patient cell lines P1 and P2 showed an additional larger band corresponding to a mutant allele. CAG repeat length in NPCs was evaluated at varying passages (indicated by p13, p15 or p17).



849  
850  
851  
852  
853  
854  
855  
856

**Figure S-1.3:** Transcriptional changes in SCA7 patient-derived fibroblasts (n=2), compared to unaffected control fibroblasts (n=1). All levels shown relative to β-actin and unaffected control cells.

Individual code	CAG genotype	Age at diagnosis	Age at biopsy	iPSC codes
-----------------	--------------	------------------	---------------	------------

P1	10/47	37	50	P1a
P2	10/41	44	44	P2a P2b
C1	10/10	n/a	33	C1a C1b

857  
858  
859  
860

**Table S-1.1:** SCA7 patient and unaffected control cell lines, genotypes and ages

**Primary antibodies**

Antibody	Full name	Species	Supplier	Dilution
AFP	Alpha-fetoprotein	Mouse	Abcam	1:100
ASA	Anti-sarcomeric alpha actinin	Rabbit	Abcam	1:100
ATXN7	Ataxin 7	Rabbit	Thermo Scientific	1:400
CRX	Cone-rod homeobox	Sheep	R&D Systems	1:20
FOXA2	Forkhead box A2	Rabbit	Abcam	1:1000
GABA	$\gamma$ -aminobutyric acid	Rabbit	Sigma-Aldrich	1:500
GFAP	Glial fibrillary acidic protein	Rabbit	Abcam	1:100
NES	Nestin	Mouse	Abcam	1:1000
NP	Nucleocapsid protein of Sendai virus	Mouse	Gift from Mahito Nakanishi	1:1500
OCT4	POU class 5 homeobox 1	Rabbit	Abcam	1:200
RCVRN	Recoverin	Rabbit	Millipore	1:1000
SMA	Smooth muscle actin	Mouse	Abcam	1:100
TRA-1-60 (PODXL) Alexa-488 conjugated	Podocalyxin like	Mouse	Millipore	1:200
$\beta$ III-Tubulin	Tubulin, beta 3 class III	Mouse	Abcam	1:300

861  
862

**Secondary antibodies**

Antibody	Dye	Species	Supplier	Dilution
Anti-sheep	Alexa-488	Donkey	Jackson ImmunoResearch	1:500
Anti-rabbit	Cy3	Donkey	Jackson ImmunoResearch	1:500
Anti-mouse	Alexa-488	Goat	Jackson ImmunoResearch	1:500

863  
864  
865  
866  
867  
868  
869  
870  
871

**Table S-1.2:** Antibodies for immunocytochemistry

Gene	Primer	Sequence (5' to 3')*
ATXN7	Atxn7 CAG RNA F	HEX-CGAGCTTTCAGAATGCAGC
	Atxn7 CAG RNA F	CACTTCAGGACTGGGCAGAG
B-ACTIN	FORWARD	Proprietary Primer Design UK
	REVERSE	Proprietary Primer Design UK
NANOG	FORWARD	CAGCCCCGATTCTTCCACCAG
	REVERSE	CGGAAGATTCCCAGTCGGGTT
SOX2	FORWARD	GGGAAATGGGAGGGGTGCAAA

	REVERSE	TTGCGTGAGTGTGGATGGGAT
OCT3/4	FORWARD	GACAGGGGGAGGGGAGGAGC
	REVERSE	CTTCCCTCCAACCAGTTGCC
MITF	FORWARD	TTCACGAGCGTCCTGTATGCAGAT
	REVERSE	TTGCAAAGCAGGATCCATCAAGCC
NRL	FORWARD	GGTCCTAGTCCCAGCTCTTC
	REVERSE	TCGTCCAATCCACATGAGAATTA
OTX2	FORWARD	TGCAGGGGTTCTTCTGTGAT
	REVERSE	AGGGTCAGAGCAATTGACCA
PAX6	FORWARD	CGGAGTGAATCAGCTCGGTG
	REVERSE	CCGCTTATACTGGGCTATTTTGC
RCVRN	FORWARD	CCAGAGCATCTACGCCAAGT
	REVERSE	CACGTCGTAGAGGGAGAAGG
RHO	FORWARD	GTCGATTCCACACGAGCACTG
	REVERSE	CCTCTCTGAATGGATACTTCGTC
RPE65	FORWARD	GCCCTCCTGCACAAGTTTGACTTT
	REVERSE	AGTTGGTCTCTGTGCAAGCGTAGT
ARR3	FORWARD	TCACTTCCAAGTCATCACGG
	REVERSE	GGTGTTCCTGGTTGATCC
GNAT1	FORWARD	TAGCTGAGGGGAGTGCAAT
	REVERSE	CCTCAAAGACTGTGGCCTCT

873

ATXN7	FORWARD	GCCAGCCGTGAACAATGTC
	REVERSE	TTCCTCCCCGTGCTATTTTCA
BEX1	FORWARD	GGAGGAGACTACAAGGATAGG
	REVERSE	TCCTTTTCTTCATTTTCTTGTT
DNAJA1	FORWARD	AAAGGAGGAGAACAGGCAATTAA
	REVERSE	TAGGGTACTGAGAGCTGATGT
GRIA2	FORWARD	CTATGGCATCGCAACACCTAA
	REVERSE	GTCCTTGGCTCCACATTCAC
HSP27	FORWARD	ACGAGCTGACGGTCAAGAC
	REVERSE	GGGGGCAGCGTGTATTTCC
HSP70	FORWARD	ATGGAATCTATAAGCAGGATCT
	REVERSE	CACATACAGAACTTGATAAGC
HSP105	FORWARD	CCCGTCAGTCATATCATTTGGA
	REVERSE	AATCTTTTGAAGTTAGACACCGTATT
OLIG1	FORWARD	GTTTGGAGAGCTGTATTTAAGACT
	REVERSE	TTCTAAGAAACCCCAAGGATTTA
UCHL1	FORWARD	TGAAGCAGACCATTGGGAAT
	REVERSE	TGTTTCAGAACTGATCCATCCT
PLCB3	FORWARD	CCTTGGAATCTTTGAGCGGTTC
	REVERSE	ACTTCGTTGAGTCTCGGGTC

**Table S-1.3:** Primer sequences

874

875

876